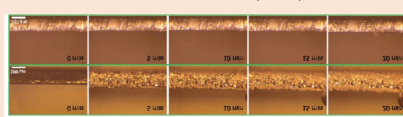
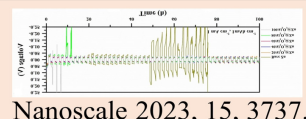


# Stabilizing Zn Anodes with Interfacial Engineering for Aqueous Zinc-ion Batteries

Wen Lu<sup>+</sup>,<sup>[a]</sup> Yingbo Shao<sup>+</sup>,<sup>[b]</sup> Ruiqiang Yan,<sup>[c]</sup> Yijun Zhong,<sup>[a]</sup> Jiqiang Ning,<sup>[d]</sup> and Yong Hu\*<sup>[e]</sup>

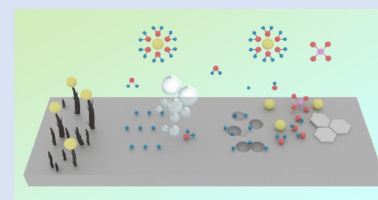
## Interfacial Engineering Strategies to Stabilize Zn Anodes for Aqueous Zinc-ion Batteries



Analytical  
techniques



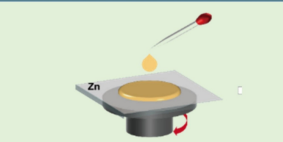
Issues



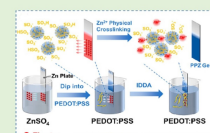
## Methods of Interfacial modification



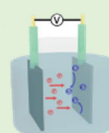
Chin. Chem. Lett.  
2023, 34, 108424.



Nano Lett. 2022, 22, 9062.



ACS Appl. Mater. Interface  
2023, 15, 31867.



Adv. Mater.  
2021, 33, 2007388.

Doctor blading  
method

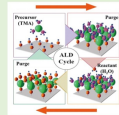
Spin-coating  
method

Chemical  
solution  
deposition

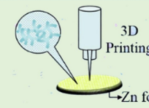
Electrochemical  
deposition



Adv. Mater.  
2021, 33, 2105951.



Nanoscale 2023, 15, 3737.



Chem. Eng. J.  
2021, 403, 126425.



Adv. Mater.  
2023, 35, 2205206.

Vapor deposition

Atomic/molecule  
layer deposition

3D printing

Vacuum freezing  
drying method

Aqueous zinc-ion batteries (ZIBs) have been regarded as a promising candidate for the next-generation energy-storage devices due to their intrinsic safety, low cost, resource abundance, and environmental friendliness. Nevertheless, the commercial applications of ZIBs have been largely plagued by the instability of the Zn anodes. Interfacial engineering arises as a straightforward and effective method to address the instability issues for the development of high-performance ZIBs. In this review, a comprehensive overview of recent progress and perspective in interfacial engineering techniques to stabilize

Zn anodes in ZIBs is presented. With emphasis on the critical issues regarding the instability problems, including Zn dendrites, hydrogen evolution reaction (HER), corrosion and passivation, the major effects and the underlying mechanisms are analyzed, and the corresponding interfacial engineering strategies as well as analytical technologies are summarized. The existing challenges and opportunities in interfacial engineering are also prospected for the future development of high-performance ZIBs.

## 1. Introduction

The growing energy demands of modern society have spurred the development of advanced energy storage devices.<sup>[1]</sup> Among the various energy storage systems, lithium-ion batteries (LIBs) have dominated the energy markets for decades due to their remarkable characteristics, including high energy density, lightweight design, and extended cycle life.<sup>[2]</sup> Despite succeeding in mass production, limited lithium resources, high cost, and safety concerns impede their broader application.<sup>[3]</sup> In response to these challenges, Zn-ion batteries (ZIBs) have emerged as promising alternatives to traditional LIBs by features of the low redox potential ( $-0.76$  V versus SHE), a high theoretical specific capacity ( $820 \text{ mAh g}^{-1}$ ), abundant reserve and intrinsic safety.<sup>[4]</sup> Therefore, ZIBs are expected to meet the diverse requirements of practical applications.

The configuration of ZIBs comprises of the cathode, separator, electrolyte, and anode.<sup>[5]</sup> The cathodes usually demonstrate either tunnel structures or layered structures for hosting  $\text{Zn}^{2+}$ , such as manganese-based oxides, vanadium-based oxides, Prussian blue analogues, organic composites, and Zn powder or Zn plates are generally employed as anodes.<sup>[6]</sup>

These two electrodes in  $\text{Zn}^{2+}$ -salt electrolyte are separated with a separator that prevents short circuits.<sup>[7]</sup> In the past decades, numerous efforts have been devoted to exploring cathode materials, but there are also many elusive challenges remaining in the advancement of cathode materials.<sup>[8]</sup> The bottleneck of cathodes (Mn-based composites,<sup>[9]</sup> V-based composites,<sup>[10]</sup> and Prussian blue analogs,<sup>[11]</sup> etc.) primarily lies in dissolution of active materials, unstable structures, strong electrostatic interactions, and intrinsically low electronic conductivity. The unstable structures of the cathodes trigger structural degradation, leading to poor cycling performance, while the dissolution of active materials accelerates rapid capacity fading. Moreover, the strong electrostatic interactions between host materials and bivalent  $\text{Zn}^{2+}$  result in low  $\text{Zn}^{2+}$  diffusion coefficients. Particularly, composites, such as Mn-based composites, V-based composites and Prussian blue analogs, experience dissolution during cycling, leading to capacity fading.<sup>[12]</sup> Addressing these issues are crucial for the progress in ZIB cathode materials. Nevertheless, the industrialization of ZIBs is still restricted, which can be attributed to the deficiency of high-performance Zn anode and understanding of mechanisms. Similar to LIBs, ZIBs, as a “rocking chair battery”, rely on the transport of  $\text{Zn}^{2+}$  between the anode and cathode to realize the energy storage.<sup>[13]</sup> It is worth noting that  $\text{Zn}^{2+}$  executes plating/stripping at the anode surface during the charge/discharge process, which exerts a significant influence on the coulombic efficiency (CE) and stability of the ZIBs.<sup>[14]</sup> Unfortunately, the deposition and stripping of  $\text{Zn}^{2+}$  are generally accompanied with the formation of Zn dendrites, hydrogen evolution reaction (HER), corrosion and passivation, being significant bottlenecks to the commercialization of ZIBs.<sup>[15]</sup> It is imperative to overcome these challenges for the development of high-performance ZIBs.

The above issues are closely related to the interface between electrolyte and Zn anodes.<sup>[16]</sup> To alleviate these issues, significant efforts have been made in this area, including interfacial engineering, structural design, and novel separators.<sup>[17]</sup> Interfacial engineering stands out among various strategies for enhancing Zn anodes due to its multiple advantages.<sup>[4a]</sup> In contrast to structural design and novel separators, interfacial engineering provides a more versatile approach.<sup>[5b,8a]</sup> It allows for the use of standard materials like Zn foil and commercial separators, enhancing both practicality and cost effectiveness.<sup>[10,11,12]</sup> Moreover, compared to single method, interfacial engineering encompassing surface coating and the electrolyte design, can be

[a] *W. Lu,<sup>†</sup> Prof. Y. Zhong*

*Key Laboratory of the Ministry of Education for Advanced Catalysis Materials  
Department of Chemistry  
Zhejiang Normal University  
321004 Jinhua (China)*

[b] *Y. Shao<sup>†</sup>*

*College of Geography and Environmental Science  
Zhejiang Normal University  
321004 Jinhua (China)*

[c] *Dr. R. Yan*

*School of Pharmaceutical and Chemical Engineering  
Taizhou University  
318000 Jiaojiang (China)*

[d] *Prof. J. Ning*

*Department of Optical Science and Engineering  
Fudan University  
200438 Shanghai (China)*

[e] *Prof. Y. Hu*

*College of Chemistry and Materials Engineering  
Zhejiang A&F University  
311300 Hangzhou (China)  
E-mail: yonghu@zafu.edu.cn  
yonghu@zjnu.edu.cn*

*Homepage: http://yonghu.zjnu.edu.cn/*

[+] *These authors contributed equally to this work.*

tailored to simultaneously address multiple challenges, such as dendrite growth, side reactions, and cycle life, resulting in a more holistic and effective solution.<sup>[13a,15a]</sup> This makes interfacial engineering a promising strategy for advancing the practical applications of Zn anodes in various energy storage systems.<sup>[18]</sup> Among these strategies, interfacial engineering represents one of the most straightforward and attractive methods to induce the even deposition behavior of  $Zn^{2+}$ , effectively alleviating Zn dendrites and side reactions.<sup>[19]</sup> Moreover, interfacial engineering exhibits its unique advantages in terms of simplicity and high efficiency, making it a promising candidate for large-scale energy storage systems.<sup>[19f]</sup> Previous reviews are primarily focused on protective materials to stabilize Zn anodes.<sup>[17,18,20]</sup> Although it is pivotal to explore artificial layer materials for proceeding the Zn anodes, the actual effectiveness of protection is also constrained by the interfacial engineering strategies.<sup>[21]</sup> Due to the unique properties of the designed interface materials, selection of an appropriate construction technique is essential for applying these modified materials to the Zn anodes. There is an emergency to

emphasize the vital connection between material properties and interfacial engineering strategies in advancing ZIBs.

In this review, we present a comprehensive overview of the interfacial engineering strategies for dendrite-free Zn metal anodes (Scheme 1). The issues and their fundamental mechanisms of the Zn anodes for aqueous ZIBs are first introduced. Subsequently, recent advancements in various interfacial engineering methods and analytical technologies are summarized. Finally, the prospects and directions of the ZIBs are proposed to deepen the research in this field.

## 2. Issues in Zn Metal Anodes

Despite the various merits of Zn anodes, they still face some inherent challenges, which limit the scale-up implementation of ZIBs (Figure 1a). Based on many research studies, it is acknowledged that the Zn anode-related issues principally stem from the dendrite formation, HER, corrosion, and passivation, which will be analyzed in detail in this section.



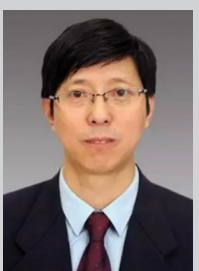
Wen Lu received her M. S. degree in Chemistry from Zhejiang Normal University (ZJNU) in 2020. She joined ZJNU in 2020 as a research assistant. Her research interests are mainly focused on electrode materials for energy storage and conversion devices.



Yingbo Shao graduated from Huaqiao University in 2022. Now, he is a M. D. student in Prof. Yong Hu's group at Zhejiang Normal University. His research interests are synthesis of electrode materials for aqueous Zn-ion batteries.



Ruiqiang Yan received his B.S. degree in 2001 and Ph. D. degree in 2006 from the University of Science and Technology of China (USTC). He is currently an Associate Professor in School of Pharmaceutical and Chemical Engineering, Taizhou University. His research interests are on electrochemistry in nanostructured semiconductors and solid state oxide fuels (SOFC).



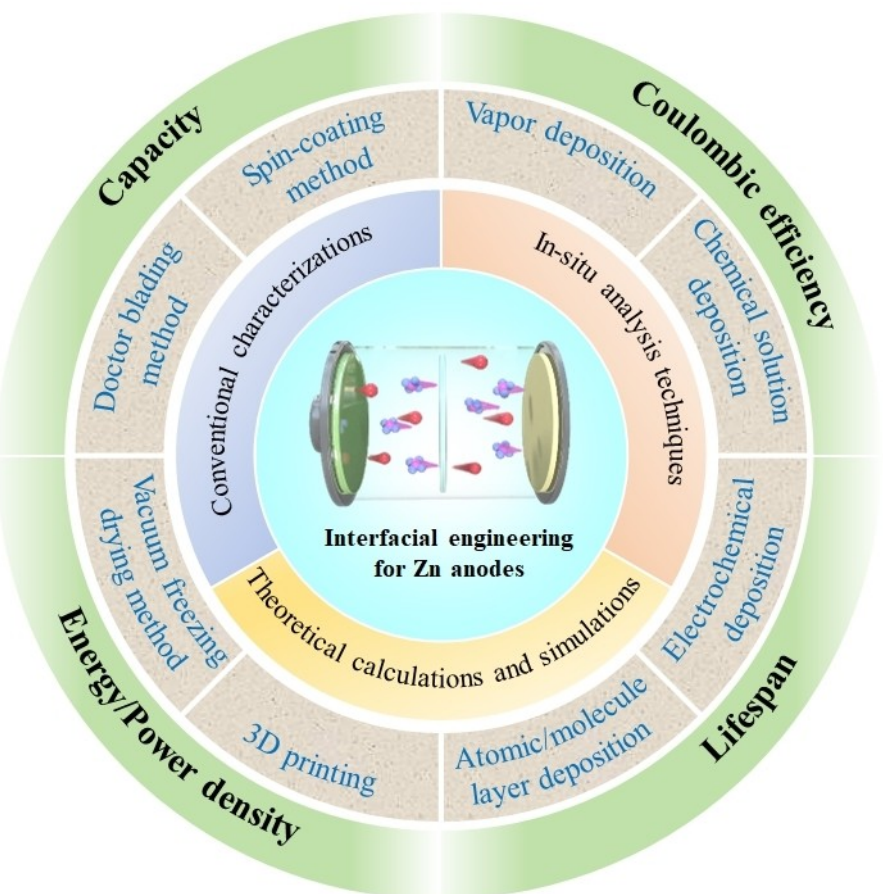
Yijun Zhong is a Full Professor at the College of Chemistry and Materials Science, Zhejiang Normal University (ZJNU), China. He joined ZJNU in 1983 and is a visiting fellow at Institution of Catalysis, Zhejiang University for two years. He received his Ph.D. degree in Industrial Catalysis from Zhejiang University of Technology, China in 2008. His research interests include the design and application of inorganic nanostructures for industrial catalysis and energy conversion and storage.



Jiqiang Ning received his B. S. degree in 2000 and M. E. degree in 2003, both from the University of Science and Technology of China (USTC), and his Ph. D. degree in 2007 from the University of Hong Kong (HKU) where he then worked as a postdoctoral researcher in the lab of laser spectroscopy at the Physics Department. He is currently a professor at the Department of Optical Science and Engineering, Fudan University, and his current research is focused on optical spectroscopic studies on non-linear optical phenomena, electronic behaviors and defect states in semiconductors and their nanostructures.



Yong Hu obtained his Ph. D. degree in inorganic Chemistry in 2006 at University of Science and Technology of China (USTC). He then worked as a research fellow at Nanyang Technological University (NTU). From 2008 to 2023, he worked as a full professor at the College of Chemistry and Life Science, Zhejiang Normal University. In 2023, he joined Zhejiang A&F University as a full professor at the College of Chemistry and Materials Engineering. His current research interests are focused on the design and synthesis of nano-materials for energy and environmental applications.



**Scheme 1.** Interfacial engineering strategies for stabilizing Zn anodes.

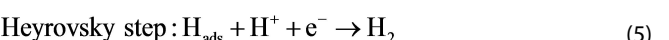
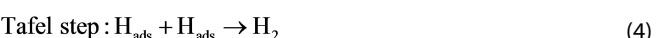
It is widely accepted that Zn electrodeposition tends to form dendrites, which is a major and critical issue in ZIBs.<sup>[22]</sup> Dendrite growth is closely associated with the inhomogeneous deposition of Zn caused by the uneven distribution of electric field and concentration gradient.<sup>[23]</sup> In theory, nucleation sites are randomly distributed on the surface of the Zn anode, but in the real case of pristine Zn foil or electroplated Zn, the surface is not atomically smooth, which results in an inhomogeneous electric field distribution and nucleation barriers, and  $Zn^{2+}$  thermodynamically tends to form nuclei at sites with lower energy barriers during the initial nucleation process.<sup>[24]</sup> These  $Zn^{2+}$  subsequently prefer to deposit at the initial nucleus, gradually growing into protrusions (Figure 1b).<sup>[25]</sup> The tips of these protrusions exhibit greater curvature, resulting in a higher surface charge density, thereby stimulating stronger local electric field intensity.<sup>[26]</sup> Due to the “tip effect”, lots of  $Zn^{2+}$  are inclined to deposit on these tips, eventually leading to the growth of larger dendrites.<sup>[27]</sup> These loose dendrites attached to the substrate can peel off to form “dead” Zn, resulting in poor coulombic efficiency (CE) and inferior capacity of the battery.<sup>[28]</sup> More seriously, the dendrite growth can easily penetrate the separator, causing battery failure via a short circuit.<sup>[29]</sup>

Apart from the dendrite issue, HER caused by water in the electrolyte is another issue in the application of ZIBs.<sup>[30]</sup> As shown in Figure 1(c), the equilibrium potential of  $H_2O/H_2$  is

higher than that of  $Zn^{2+}/Zn$  across the whole pH range, signifying that the coexistence of Zn and  $H_2O$  is thermodynamically unstable.<sup>[31]</sup> Their reactions are displayed as follows:



During the Zn plating process, hydrogen evolution and Zn deposition are competitive reactions. The HER is thermodynamically preferred over Zn deposition during the plating process. In spite of this, it also considers the kinetic factors associated with the HER in the practical ZIBs.<sup>[32]</sup> Generally, the HER process in ZIBs can be divided into two sequential steps: the Volmer step and the Tafel step or the Heyrovsky step, as follows:



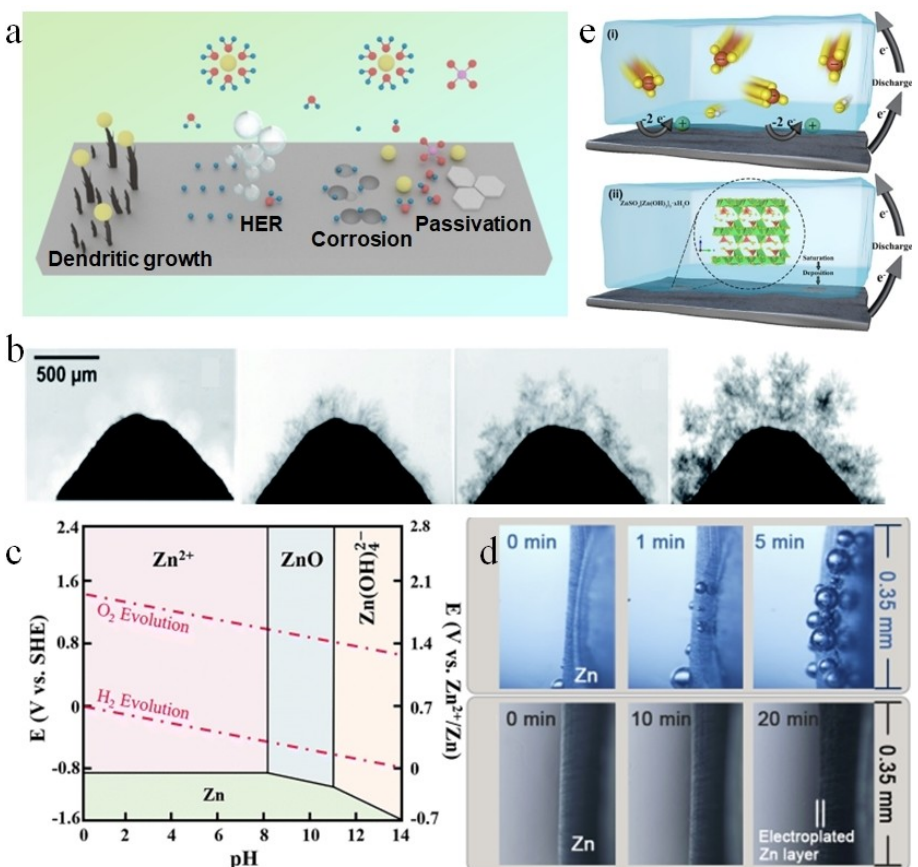
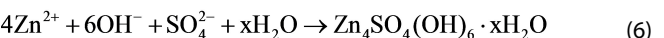


**Figure 1.** a) Schematic illustration of the present challenges associated with the Zn anode in ZIBs. b) Operando study of Zn dendrite growth, dissolution, and regrowth in aqueous electrolytes. Reproduced from ref. [25] Copyright (2018), with permission from Elsevier. c) Pourbaix diagram of the Zn metal in aqueous solution. Reproduced from ref. [31] Copyright (2016), with permission from Elsevier. d) In situ optical microscopic images of hydrogen evolution in mild acidic electrolyte. Reproduced from ref. [36] Copyright (2018), with permission from Elsevier. e) Schematic diagram of  $ZnSO_4 \cdot [Zn(OH)_2] \cdot xH_2O$  formation on anode surface. Reproduced from ref. [39] Copyright (2020), with permission from Wiley-VCH.

For HER on Zn anode, the  $H_{ads}$  generated in the Volmer step is a rate-limiting step.<sup>[33]</sup> According to the Tafel equation:  $\eta = b \log i + \alpha$  ( $\eta$  represents the HER overpotential,  $b$  is Tafel slope, which is also a constant value,  $i$  indicates the current density,  $\alpha$  implies the constant value). The high Tafel slope is approximately 0.12 V and the constant  $\alpha$  for Zn metal is about 1.24 V, which results in a high overpotential, decreasing the actual HER potential below the equilibrium potential of  $Zn^{2+}/Zn$ .<sup>[34]</sup> Taking this into consideration, Zn metal anode exhibits a high HER overpotential, which is unfavorable for hydrogen evolution kinetics. Therefore, the HER kinetics is limited to some extent. Moreover, external factors, such as system perturbations and temperature changes, can also influence the degree of reduction for the hydrogen evolution overpotential.<sup>[35]</sup> However, the  $H_2$  can still gradually generate and accumulate in the cells (Figure 1d).<sup>[36]</sup> The continuous generation of  $H_2$  can elevate the internal pressure of the battery, which leads to bulging and electrolyte leakage, ultimately resulting in a reduced lifespan.<sup>[37]</sup>

The corrosion is inseparable from HER, which has attracted long-term attention. When Zn metal directly contacts with the electrolyte, it leads to chemical corrosion and electrochemical corrosion.<sup>[18]</sup> During the electrochemical processes, various microscale primary batteries are formed at the interface of

electrolyte/Zn metal, leading to the corrosion of Zn and the evolution of  $H_2$ .<sup>[36,38]</sup> Along with the consumption of  $H^+$ ,  $OH^-$  continuously concentrates on the surface of Zn anode, causing local pH change and forming a local alkaline environment, which results in insulative by-products like  $Zn_4SO_4(OH)_6 \cdot xH_2O$  (Figure 1e).<sup>[39]</sup>



Unlike LIBs, it is difficult to construct an in-situ functional solid-electrolyte interphase (SEI) on Zn anodes in aqueous electrolyte systems, instead of the loose and unstable by-products accumulated, indicating that the corrosion will not be terminated and the aqueous electrolyte still can penetrate the passivated layer to react with the interior Zn metal.<sup>[40]</sup> Consequently, the Zn metal and electrolyte are irreversibly consumed, leading to increased interfacial resistance, inferior CE, and thus affecting the lifespan.<sup>[41]</sup>

In fact, the growth of dendrites, HER, corrosion and passivation are inseparable, which interact with each other. The formation of Zn dendrites leads to the increment of the contact area between the electrolyte and the Zn anode, which triggers the HER.<sup>[42]</sup> The occurrence of HER causes local pH fluctuations,

leading to an elevation in  $\text{OH}^-$  concentration, which, in turn, accelerates the corrosion process and results in the formation of by-products on the anode surface.<sup>[21,43]</sup> These by-products account for uneven distribution of electric field on the electrode surface, consequently promoting the formation of dendrites.<sup>[44]</sup>

Cross talk indicates a process where byproducts generated at one electrode traverse the separator toward the other electrode, triggering undesirable side reactions.<sup>[45]</sup> This phenomenon is observed in many batteries, such as Zn–I<sub>2</sub>, Zn–Br<sub>2</sub>, Zn–S batteries. Taking Zn–I<sub>2</sub> battery as an example, on the cathode side, the I<sub>2</sub> is electrochemically reduced to I<sup>–</sup> during discharge process, accompanied by the formation of soluble polyiodides. The migration of polyiodides from the electrode to the electrolyte leads to overcharge and the consumption of active materials. Due to the concentration gradient, these polyiodides may permeate the separator to the Zn anode, and then further react with the Zn anode, resulting in the self-discharge phenomenon and severe Zn corrosion.<sup>[46,47]</sup> Consequently, specific capacity and CE experience significant reductions. Moreover, the corrosion-induced uneven surface on the Zn anode may disrupt the homogeneous deposition of Zn, promoting HER and passivation. On the anode side, Zn dendrite formation and parasitic side reactions during cycling can detrimentally cross talk to the cathode. The generated H<sub>2</sub> at the anode is reported to increase the impedance and expedite capacity decay of the cathodes.<sup>[48]</sup> Therefore, it is urgent to propose some comprehensive strategies to simultaneously alleviate above issues.

### 3. Operation Method and Process of Modified Zinc Anode

As mentioned above, it is imperative to develop protective strategies for achieving a highly reversible Zn anode. Interfacial engineering, as a promising strategy, can effectively restrict the dendrite growth and side reactions.<sup>[44b,49]</sup> Meanwhile, numerous coating materials, such as polymers, metals, carbon-based materials and composites, can serve as the protective layers for surface modification of the Zn anode, leading to an enhancement of the lifespan and CE.<sup>[19f,50]</sup> Therefore, selecting an appropriate method to specific materials plays a pivotal role in the preparation of high-quality coatings. This section summarizes and discusses recent advancements in interfacial engineering strategies for Zn anode.

#### 3.1. Doctor blading method

The doctor-blading is a straightforward method for modifying Zn anodes to enhance the stability. This method involves a simple operation process, where binders and coating materials are mixed in an organic solvent to form a slurry. Subsequently, the slurry is cast onto Zn foils, and upon solvent evaporation, a protective film is formed on the Zn anode surface. The preparation process of the films can be precisely controlled by

some parameters, such as blade rate, slurry density and blade thickness.<sup>[51]</sup> Furthermore, it is versatile and adaptable to a wide range of coating materials, including carbon-based materials, metal-based materials, polymers and so on.<sup>[52]</sup> For example, Wu et al. successfully constructed a compact poly(vinylidene fluoride) (PVDF)-Zn(TFSI)<sub>2</sub> coating (Zn@PZ) for modifying Zn anodes (Figure 2a).<sup>[53]</sup> To evaluate the effects of Zn(TFSI)<sub>2</sub> on the coating layer, different mass ratios of PVDF and Zn(TFSI)<sub>2</sub> (4:0, 4:3, 4:4 and 4:5) were prepared (labeled as Zn@PZ40, Zn@PZ43, Zn@PZ44 and Zn@PZ45). The Zn@PZ44 exhibited superior characteristics with lower charge transfer impedance and higher ionic conductivity than those of Zn@PZ40, Zn@PZ43, and Zn@PZ45, effectively accelerating the transport of Zn<sup>2+</sup> (Figure 2b and c). However, it was worth noting that an increase in Zn(TFSI)<sub>2</sub> content led to a decrease in mechanical strength (Figure 2c). Therefore, the PZ44 was the optimal coating with a balance between mechanical strength and ionic conductivity, which partially isolated the Zn anode from the electrolyte, ensuring a more uniform Zn<sup>2+</sup> flux, thus inhibiting dendrite growth and side reactions (Figure 2d). Mao et al. constructed a free hydroxyl-rich guar gum (RFH-GG) film by a common doctor blading method to inhibit side reactions and dendrite growth (Figure 2e).<sup>[54]</sup> Specifically, the abundant hydroxyl groups of the RFH-GG played a crucial role in regulating the solvated structure of Zn<sup>2+</sup>, which resulted in a reduced content of free water at the interface, therefore decreasing the contact area between the Zn anode and free water molecules (Figure 2f). As a result, the diffusion of Zn<sup>2+</sup> through the RFH-GG coating layer remained stable within the 40 s, whereas the bare Zn anode kept increasing beyond 400 s, suggesting that the RFH-GG coating layer significantly shortened the 2D planar diffusion process, which was favorable for engineering a uniform layer and suppressing the growth of Zn dendrites (Figure 2g). Therefore, the RFH-GG@Zn symmetric cell demonstrated an exceptionally long lifespan of 2500 h at 3 mA cm<sup>–2</sup> (Figure 2h).

Briefly, the doctor blading technique is a commonly used approach for coating Zn anodes due to its low cost, simple operation and scalability for large-scale production. However, it is worth noting that this method may suffer from poor mechanical properties, leading to degradation of the lifespan, particularly at high current densities.

#### 3.2. Spin-coating method

The spin-coating represents another solution casting method to obtain relatively thin layers. Similar to the doctor blading method, it relies on solvents and adhesives to produce high-quality coatings. A typical spin-coating procedure includes four fundamental steps: solution deposition, high-speed spinning, solvent evaporation and spin off.<sup>[55]</sup> Specifically, the pre-configured slurry is first dropped onto the substrate, and then uniformly spread across the surface by the centrifugal force. Finally, the protective layer is obtained when the solvent evaporates. The thickness of a film inversely correlates with the square root of the rotation speed and the cube root of the

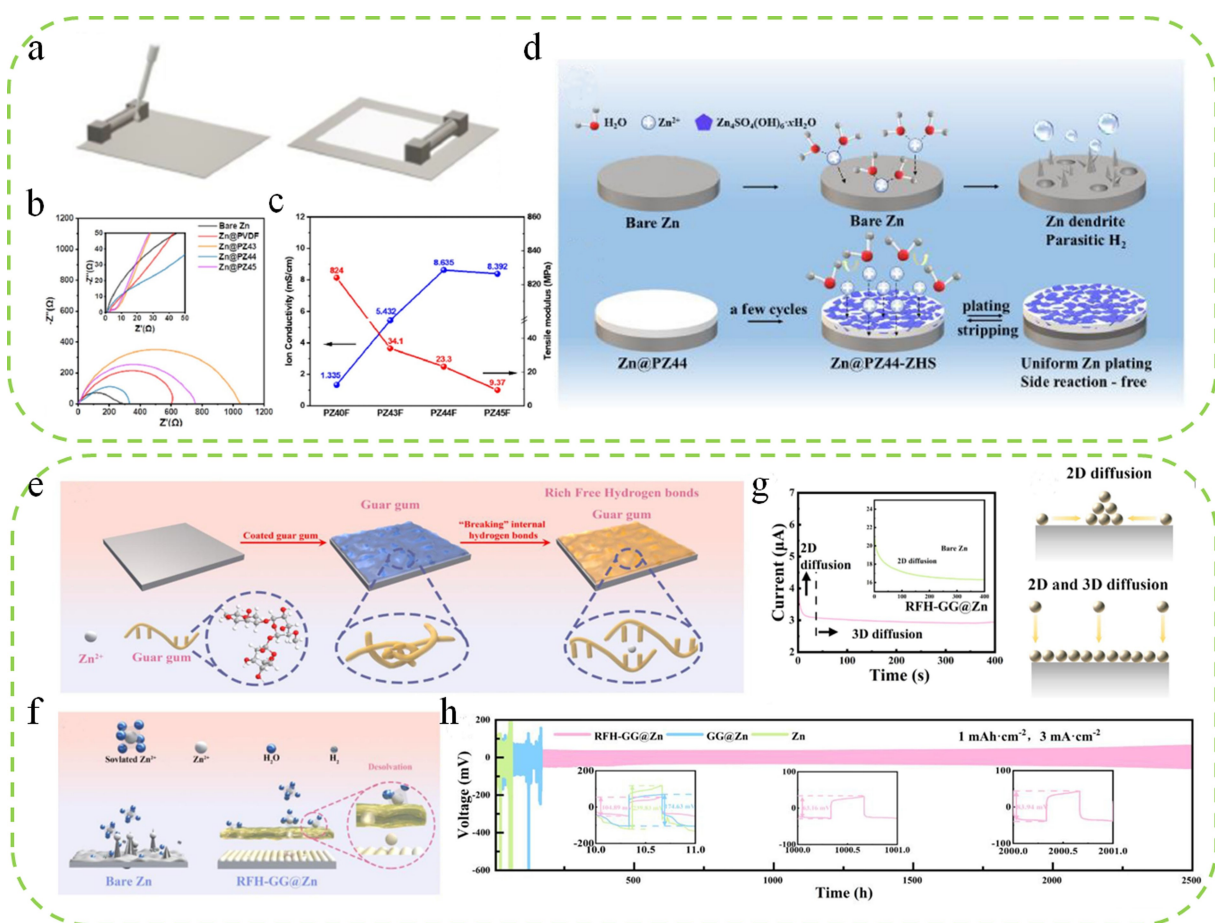


**Figure 2.** a) Fabrication procedures of the Zn@PZ. b) EIS spectra of the Zn symmetric cells before cycling at room temperature. c) The calculated ionic conductivity and tensile modulus of different coating layers. d) Schematic illustration of the surface chemistry on Zn anodes. Reproduced from ref. [53] Copyright (2023), with permission from Elsevier. e) Schematic diagram of building the RFH-GG coating. f) Schematic diagram of Zn<sup>2+</sup> deposition on bare Zn and RFH-GG@Zn electrodes. g) CA tests of bare Zn and RFH-GG@Zn at a 20 mV overpotential and schematic diagram of the diffusion behavior of Zn<sup>2+</sup> on bare Zn and RFH-GG@Zn. h) Cycling performance of bare Zn, RFH-GG@Zn and GG@Zn symmetric cells at 3 mA cm<sup>-2</sup> for 1 mAh cm<sup>-2</sup>. Reproduced from ref. [54] Copyright (2023), with permission from Elsevier.

slurry viscosity.<sup>[55]</sup> Therefore, the vital parameters for preparation are the slurry viscosity, spin speed and time.<sup>[55]</sup> Various organic polymers and inorganic materials can be used to modify the Zn anode in this way.<sup>[56]</sup> As shown in Figure 3(a), Hieu et al. employed the spin-coating technique to prepare a highly polar  $\beta$ -phase poly(vinylidene difluoride) ( $\beta$ -PVDF) coating layer on a Zn anode ( $\beta$ -PVDF@Zn). This coating layer acted as a buffer layer to shield the Zn anode from direct contact with the electrolyte, effectively mitigating dendrite growth, suppressing side reactions and regulating the Zn<sup>2+</sup> migration behavior.<sup>[57]</sup> Clearly, the bare Zn exhibited significant dendritic growth after cycling, whereas the  $\beta$ -PVDF@Zn remained a smooth and flat surface without dendrites (Figure 3b). During the cycling, the  $\beta$ -PVDF coating played an essential role in ensuring a uniform Zn<sup>2+</sup> flux by strong interactions between the electronegative C–F functional groups and Zn<sup>2+</sup>. Furthermore, a preferable diffusion path was established by aligning the F atoms oriented in the same direction, facilitating the penetration of Zn<sup>2+</sup> and regulating Zn deposition between the Zn anode and  $\beta$ -PVDF (Figure 3c). Consequently, the  $\beta$ -PVDF@Zn symmetric cell exhibited an extended lifespan exceeding 2000 hours. Addition-

ally, a binder-free polyionic liquid (PCAVImBr) film combining rapid polymerization was proposed to stabilize Zn anodes.<sup>[58]</sup> As shown in Figure 3(d), a layer of PCAVImBr film was built on the surface of Zn anode via a spin-coating process, where the pore size of the film was finely tuned by modulating the ratio of the cross-linker and the ionic liquid, striking a balance between ion selectivity and mass transfer. The optimized PCAVImBr with a molar ratio of 7:1 demonstrated a uniform pore structure that facilitated the rapid transport of Zn<sup>2+</sup>. After being immersed in the electrolyte for seven days, the surface of the bare Zn foil was covered with white by-products, while Zn@PCAVImBr barely changed (Figure 3e). To further investigate the capability of anti-corrosion, linear polarization experiments were carried out in 2 M ZnSO<sub>4</sub> aqueous solution. As shown in Figure 3(f), Zn@PCAVImBr exhibited a lower corrosion current value of 1.44 mA cm<sup>-2</sup> than that of Zn foil (2.0 mA cm<sup>-2</sup>), indicating that the PCAVImBr coating endowed the Zn anode with good corrosion resistance. Contributed by the phase separation resulted in a uniform nuclei layer, leading to enhanced electrochemical performances of symmetric cells and Zn//Na<sub>3</sub>VO<sub>4</sub> full cells based on the modified Zn anodes.

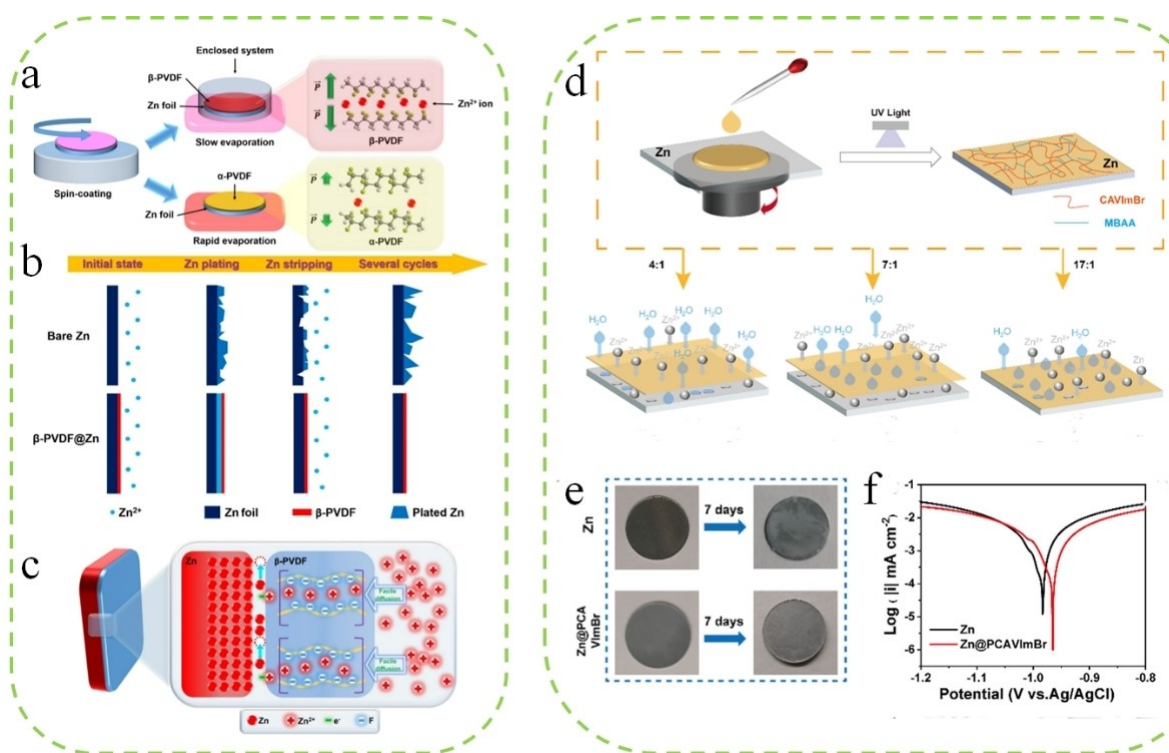


**Figure 3.** a) Schematic illustration of  $\beta$ -PVDF and  $\alpha$ -PVDF coating synthesis processes. b) Schematic demonstration of Zn stripping/plating on bare Zn anode and  $\beta$ -PVDF@Zn anode. c) Illustration of the ion distribution and uniform deposition through the  $\beta$ -PVDF membrane. Reproduced from ref. [57] Copyright (2021), with permission from Elsevier. d) Fabrication method of Zn@PCAVlmBr electrode while controlling the degree of phase separation by modulating different molar ratios of monomer and cross-linker. e) Images of Zn foil and Zn@PCAVlmBr electrode before and after immersion in 2 M aqueous  $ZnSO_4$  electrolyte for one week. f) Linear polarization curves. Reproduced from ref. [58] Copyright (2022), with permission from American Chemical Society.

In short, the spin-coating technique is a simple and less time-consuming process for modifying the Zn anode. Due to the mechanization of the spin coater, this method can easily obtain controllable thickness and high reproducibility, but unlike the doctor-blading that can be applied in a large-scale, it is only suitable for small-scale laboratory production and the utilization of raw materials is limited.

### 3.3. Chemical solution deposition

Chemical solution deposition (CSD) is a simple and straightforward method for constructing coating layers through various chemical reactions, including hydrothermal method, precipitation, polymerization, etc., which is suitable for inorganic and organic materials.<sup>[59]</sup> A film can be deposited on the substrate by placing the substrate in a specific solution and the thickness of the film can be roughly controlled by the soaking time and concentration of the solution.<sup>[55]</sup> Recently, Liu et al. prepared a polymer protective layer with  $Zn^{2+}$  selective channels on the surface of Zn foil.<sup>[43b]</sup> The Zn foil was first placed in  $ZnSO_4$  electrolyte to adsorb the  $Zn^{2+}$ , followed by immersion in a PEDOT:PSS dispersion for self-assembly (2PPZ@Zn), resulting in the construction of selective  $Zn^{2+}$  transport channels (Figure 4a). In order to verify the 2PPZ@Zn with fast  $Zn^{2+}$  transport channels, PEDOT:PSS@Zn (2PP@Zn) was prepared, whose process was similar to that of 2PPZ@Zn except for the absence

of immersing the  $ZnSO_4$  electrolyte. The color change verified the successful covering of 2PPZ on the Zn foil (Figure 4b). The optical image of bare Zn displayed metallic luster, while 2PP@Zn demonstrated light blue and 2PPZ@Zn exhibited dark blue color. The surface wettability was an important factor for Zn stripping/plating. Contact angle tests revealed that the surface wettability of 2PPZ@Zn significantly improved compared to bare Zn and 2PP@Zn, indicating the presence of 2PPZ was conducive to the permeability of the electrolyte. The abundant selective  $Zn^{2+}$  channels in 2PPZ@Zn contributed to enhanced ionic conductivity,  $Zn^{2+}$  transference number, and corrosion resistance (Figure 4c-e). As a result, symmetric cells based on 2PPZ@Zn achieved an extended cycling life of 2400 h at 3  $mA\text{cm}^{-2}$  and 1  $mA\text{h}\text{cm}^{-2}$ . Moreover, Xing et al. successfully prepared a layer of  $Zn_3(PO_4)_2 \cdot 4H_2O$  coating on the surface of Zn foil (ZP@Zn) by immersing Zn foil in a mixed solution of  $Zn(NO_3)_2 \cdot 6H_2O$  and  $(NH_4)_2HPO_4$ .<sup>[60]</sup> The as-obtained ZP@Zn with reversible proton reservoir capability enabled the dynamic equilibrium of proton, where the anionic group featured with amphoteric characteristics could be able to store protons for alleviating the HER during the charge process and release proton in the discharge for reducing by-products. To get insights into the effects of ZP coating on Zn deposition, ex-situ scanning electron microscope (SEM) images and finite element simulation were performed (Figure 4f-k). Due to an uneven distribution of the electrical field and current density, the bare Zn demonstrated mossy protuberances and eventually formed

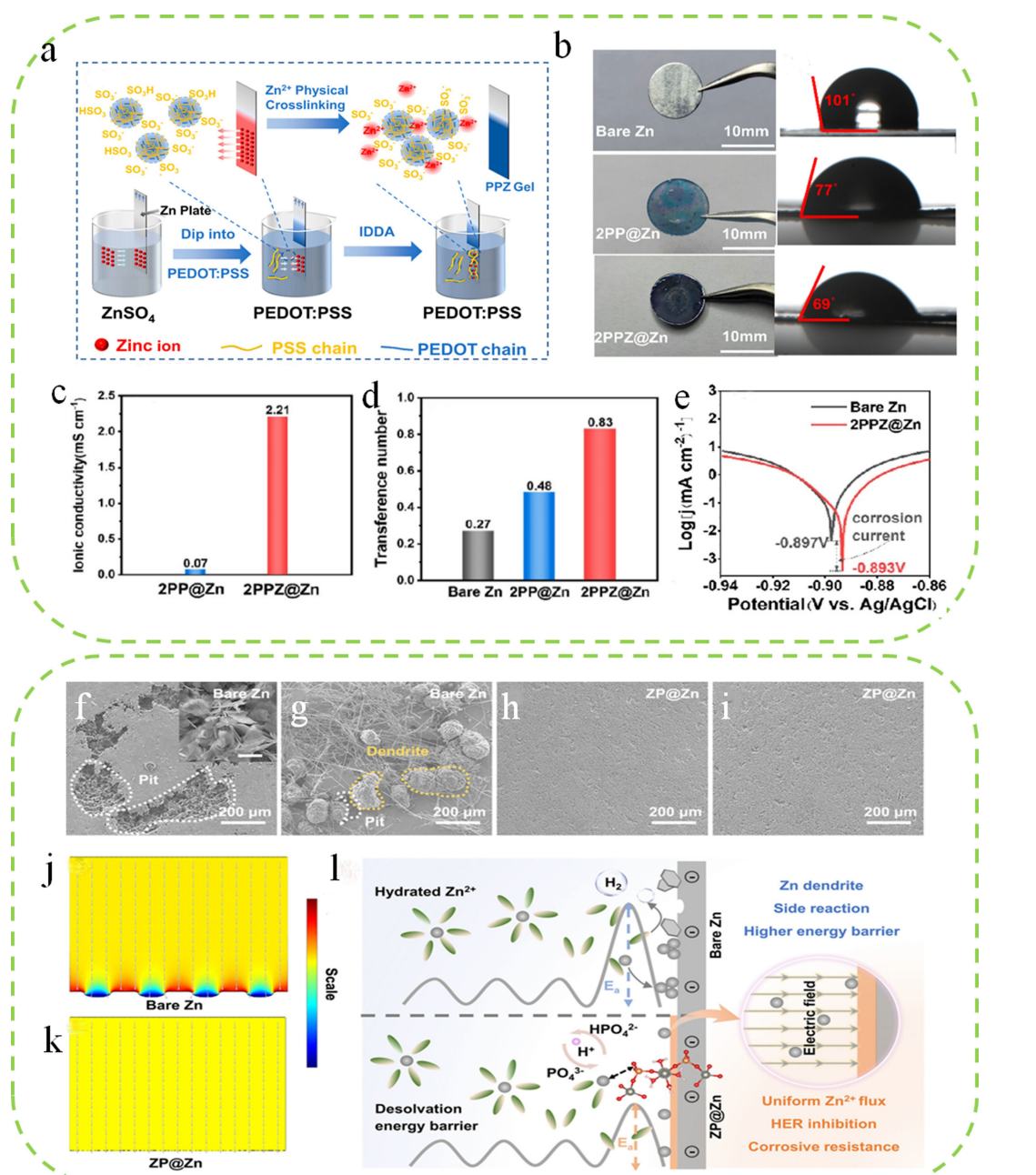


**Figure 4.** a) Schematic illustration of fabricating 2PPZ@Zn. b) Optical images of bare Zn, 2PP@Zn, and 2PPZ@Zn and electrolyte contact angles of various samples. c) Ionic conductivity of 2PP@Zn and 2PPZ@Zn. d)  $t_{\text{zn}}^{2+}$  of bare Zn, 2PP@Zn, and 2PPZ@Zn electrodes. e) Tafel plots of the bare Zn and 2PPZ@Zn anodes in the 2 M  $\text{ZnSO}_4$  electrolyte. Reproduced from ref. [43b] Copyright (2023), with permission from American Chemical Society. SEM images of bare Zn and ZP@Zn after f, h) fully discharged and g, i) fully charged in the first cycle. The simulation results of current density on j) bare Zn and k) ZP@Zn. l) Schematic illustration of the  $\text{Zn}^{2+}$  deposition processes on bare Zn and ZP@Zn. Reproduced from ref. [60] Copyright (2022), with permission from Wiley-VCH.

Zn dendrites. On the contrary, the ZP@Zn anode exhibited a flat morphology, where the ZP could induce current redistribution to favor an even deposition of  $\text{Zn}^{2+}$ . In detail, the deposition behavior could be illustrated in Figure 4(l). The ZP lowered the energy barrier for desolvation, therefore accelerating the nucleation process and the orientated electric field that prevented dendrite growth. In addition, the reversible proton storage alleviated HER and parasitic reactions.

In summary, CSD is a versatile method for constructing coating layers. The cost of the process is not involved with the

expensive equipment, which mainly comes from drugs, therefore possessing a price advantage. The in-situ formed layers with strong adhesion are not easy to peel off, which is beneficial to stabilize the Zn anode. However, it is difficult to precisely control the thickness of the coating during the reaction.

### 3.4. Electrochemical deposition

Electrochemical deposition is also carried out in a solution, which is similar to the chemical solution deposition. The key distinction between these two methods is that the latter is driven by an applied electric field.<sup>[51]</sup> The thickness of the coating can be controlled by some parameters, such as current density and deposition time.<sup>[19a,61]</sup> For instance, Yang et al. constructed 3D interconnected ZnF<sub>2</sub> as a protective layer on the surface of Zn foil in 1 M NH<sub>4</sub>F electrolyte by electrochemical

deposition, whose thickness was regulated by varying the deposition time (Figure 5a).<sup>[62]</sup> Briefly, a large amount of Zn<sup>2+</sup> was produced under a constant voltage of 15 V, subsequently reacting with the F<sup>-</sup> in the solution to form a layer of ZnF<sub>2</sub> coating on the surface of Zn foil. The as-obtained Zn@ZnF<sub>2</sub> effectively homogenized the Zn<sup>2+</sup> flux and decreased the desolvation energy barriers, endowing the Zn anodes with excellent plating/stripping stability. To further verify the above results, the electric field was evaluated with the assistance of finite element simulation to get insights into the deposition

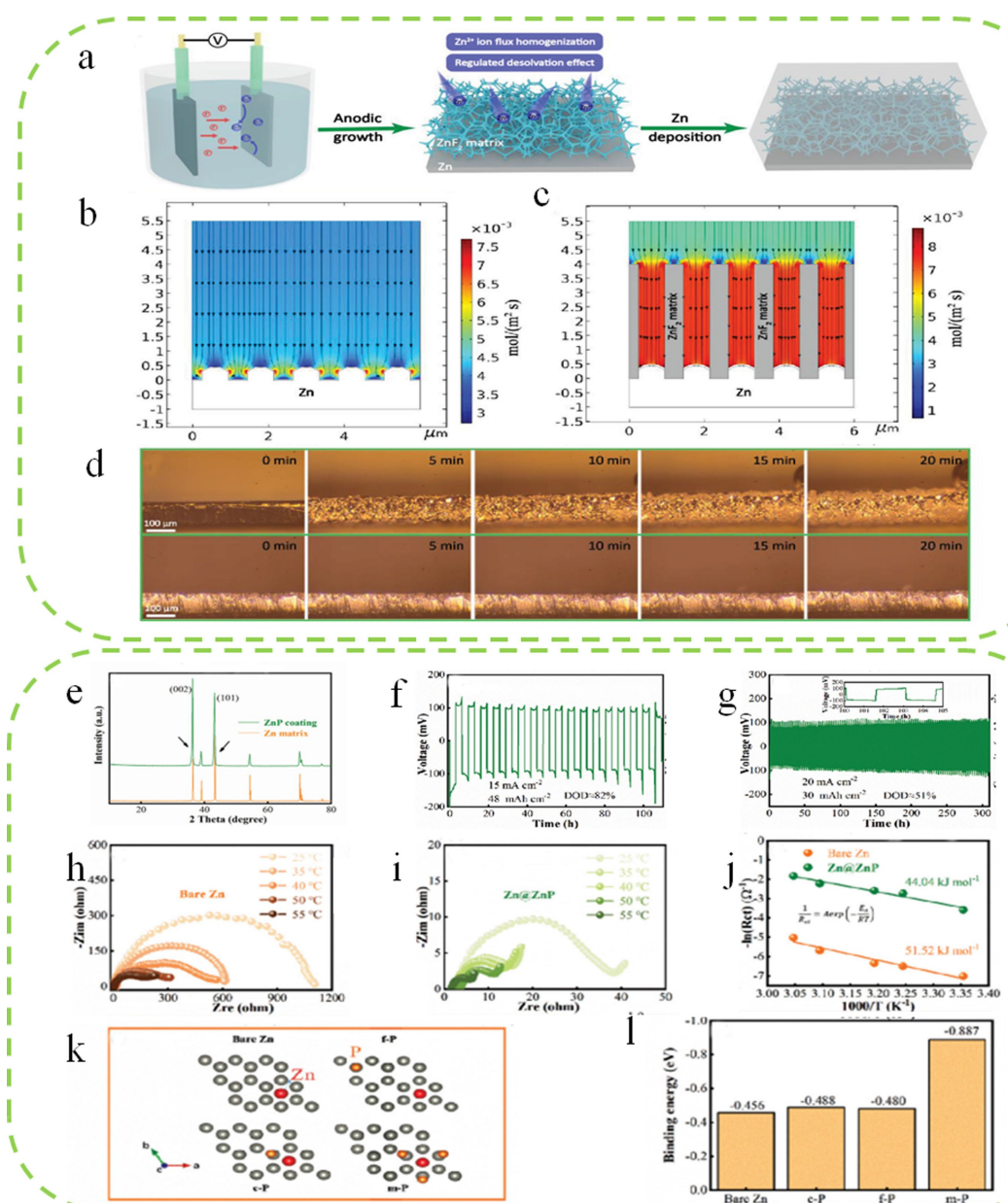


**Figure 5.** a) Schematic illustration of the fabrication of the Zn@ZnF<sub>2</sub> electrode. Numerical simulation of the Zn<sup>2+</sup> flux distribution during deposition b) on the Zn foil and c) on the Zn@ZnF<sub>2</sub> electrode. d) In situ optical observation results of the Zn deposition morphologies on the Zn foil and on the Zn@ZnF<sub>2</sub> electrode at a current density of 10 mA cm<sup>-2</sup> for 20 min. Reproduced from ref. [62] Copyright (2021), with permission from Wiley-VCH. e) GIXRD of ZnP coating and Zn matrix. Cycling performance of symmetries cell with Zn@ZnP anode at f) 15 mA cm<sup>-2</sup>/48 mAh cm<sup>-2</sup> and g) 20 mA cm<sup>-2</sup>/30 mAh cm<sup>-2</sup>. Nyquist patterns at different temperatures of the h) bare Zn and i) Zn@ZnP anode in symmetric cells. j) Arrhenius curves of bare Zn and Zn@ZnP anode. k) Zn adsorbed on bare Zn and ZnP coating at different adsorption sites, and l) the corresponding binding energy calculated by the DFT. Reproduced from ref. [63] Copyright (2021), with permission from Wiley-VCH.

behavior. The bare Zn foil exhibited an uneven distribution of  $Zn^{2+}$  flux, leading to the formation of Zn dendrites (Figure 5b). After coating a layer of  $ZnF_2$  on the surface of the Zn foil, the  $Zn^{2+}$  flux was simultaneously enhanced and homogenized, therefore achievement of uniform Zn deposition (Figure 5c). In addition, in-situ optical microscopy was applied to monitor the Zn metal electroplating process. As shown in Figure 5(d), loose particles emerged on the bare Zn foil within 5 min and gradually accumulated into notorious dendrites. Meanwhile, a small bubble was observed and kept growing into a big one after 20 min. In contrast, the surface of the  $Zn@ZnF_2$  remained flat and no dendrites or bubbles appeared. Consequently, the as-fabricated  $Zn@ZnF_2$  electrode exhibited a long lifespan of 800 h and a high CE of approximately 99.5%. To overcome the limitations of Zn anode applied in high current density and large area capacity, ZnP was electrodeposited onto Zn foil ( $Zn@ZnP$ ).<sup>[63]</sup> The grazing incidence X-ray diffraction (GIXRD) was carried out to investigate the composition of the coating, which could be seen that the diffraction peaks of  $Zn@ZnP$  were similar to the bare Zn foil (Figure 5e). It was worth noting that the diffraction peaks of  $Zn@ZnP$  shifted towards lower angles compared with the bare Zn foil, indicating the interplanar spacing was expanded. Meanwhile, the peak intensity of the (002) plane significantly enhanced with the introduction of ZnP, illustrating the (002) plane was highly exposed on the coating surface, which was conducive to the uniform deposition of  $Zn^{2+}$ . Besides, the presence of P was confirmed by X-ray photoelectron spectroscopy (XPS) and electron probe micro analyzer (EPMA) tests. To assess the cycling performances, the symmetrical cells were assembled. The symmetric cells based on  $Zn@ZnP$  revealed long-term cycling stability at  $15\text{ mA cm}^{-2}$  and  $48\text{ mAh cm}^{-2}$  under a depth of discharge (DOD)  $\approx 82\%$  and it remained stable for over 300 h even at a current density of  $20\text{ mA cm}^{-2}$  with a capacity of  $30\text{ mAh cm}^{-2}$  (DOD  $\approx 51\%$ ) (Figure 5f and g). Considering that the desolvation procedure was the rate-limiting step for  $Zn^{2+}$  deposition, the activation energy ( $E_a$ ) was calculated by the Arrhenius equation (Figure 5h–j). The  $E_a$  for the  $Zn@ZnP$  was about  $44.04\text{ kJ mol}^{-1}$ , which was lower than that of the bare Zn foil ( $51.52\text{ kJ mol}^{-1}$ ), further suggesting the existence of ZnP significantly enhanced Zn deposition kinetics and boosted  $Zn^{2+}$  transfer. To investigate the effects of the ZnP on  $Zn^{2+}$  transfer in detail, the binding energy was performed by density functional theory (DFT). The binding energy of  $Zn@ZnP$  exhibited negative than that of the bare Zn foil, regardless of the positions of P in the Zn lattice, illustrating an enhanced zincophilicity (Figure 5k and l).

In a word, the electrochemical deposition process is not involved with expensive equipment, and the preparation process is simple, easy to operate and optimized swiftly. Compared with CSD, this method can boost chemical reaction kinetics and achieve non-spontaneous reactions. This method demonstrates the prospect of industrial applications, but it is difficult to precise control the growth on the surface of Zn foil.

### 3.5. Vapor deposition

Vapor deposition is an in-situ preparation method with gaseous deposition, which makes use of physical or chemical procedures in the gas phase to construct a layer of coatings with special performances on the substrate. Based on the intrinsic nature of the process, there are two types of vapor deposition, namely physical vapor deposition (PVD) and chemical vapor deposition (CVD).<sup>[55]</sup>

Generally speaking, PVD mainly consists of two processes, namely evaporation and sputtering. These processes involve the transformation of functional coating materials from a solid target into a gaseous state, followed by physical deposition onto a substrate.<sup>[52]</sup> The thickness of the deposited layers can be precisely controlled from nanometers to hundreds of micrometers by tuning process durations from fractions of seconds to hours.<sup>[56]</sup> The types of PVD include ion beam sputtering (IBS), magnetron sputtering, arc ion plating, vacuum evaporation, molecular beam epitaxy and so on.<sup>[64]</sup> IBS, as a typical kind of PVD strategy, has been widely used in the manufacturing functional layers for various materials, particularly those with a high melting point, which usually makes use of an electric field to ionize the inert gas to produce high-energy particles.<sup>[52,64]</sup> These high-energy particles impact the target material at high velocities, then the atoms or molecules of the target material are sputtered onto the substrate.<sup>[65]</sup> As the atoms or molecules accumulate, a layer of film is gradually formed on the substrate.<sup>[65]</sup> As shown in Figure 6(a), nano-Au particles were deposited onto Zn anodes (NA-Zn-60) by IBS.<sup>[66]</sup> These deposited nano-Au particles acted as nucleation sites, inducing uniform deposition and regulating morphology evolution during Zn plating/stripping. The bare Zn foil exhibited protrusions that could pierce the separator, leading to short circuits, while the NA-Zn-60 demonstrated a smooth surface, effectively inhibiting dendrite growth and side reactions (Figure 6b). As a result, the symmetrical cell based on NA-Zn-60 displayed an extended cyclic life. Benefiting from the characteristics of high conversion efficiency, magnetron sputtering was proposed to construct coating layers. Jiang et al. prepared the  $WSe_2$ -Zn and  $MoSe_2$ -Zn anodes by magnetron sputtering (Figure 6c).<sup>[44c]</sup> With the assistance of the selenides on the Zn anodes, zincophilicity and nucleation sites were significantly improved, which strengthened the even distribution of the electric field for promoting homogeneous deposition and exfoliation of  $Zn^{2+}$  and inhibiting the generation of by-products. Yang et al. employed  $HfO_2$  as the target to prepare a coating with a spatial dielectric-metallic gradient composition (Zn-GZH) by magnetron sputtering (Figure 6d).<sup>[67]</sup> The distinctive gradient structure featured an outermost  $HfO_2$ -rich surface and a Zn-rich oxide region inside was achieved by adjusting the sputtering frequency power of the Zn and  $HfO_2$  target throughout the deposition (Figure 6e). The Zn-GZH exhibited that the outermost  $HfO_2$  reduced the tendency for HER, while the Zn and  $Zn_xHfO_y$  in the subsurface regulated the  $Zn^{2+}$  flux and guaranteed an even electric field distribution, resulting in a dendrite-free Zn anode.

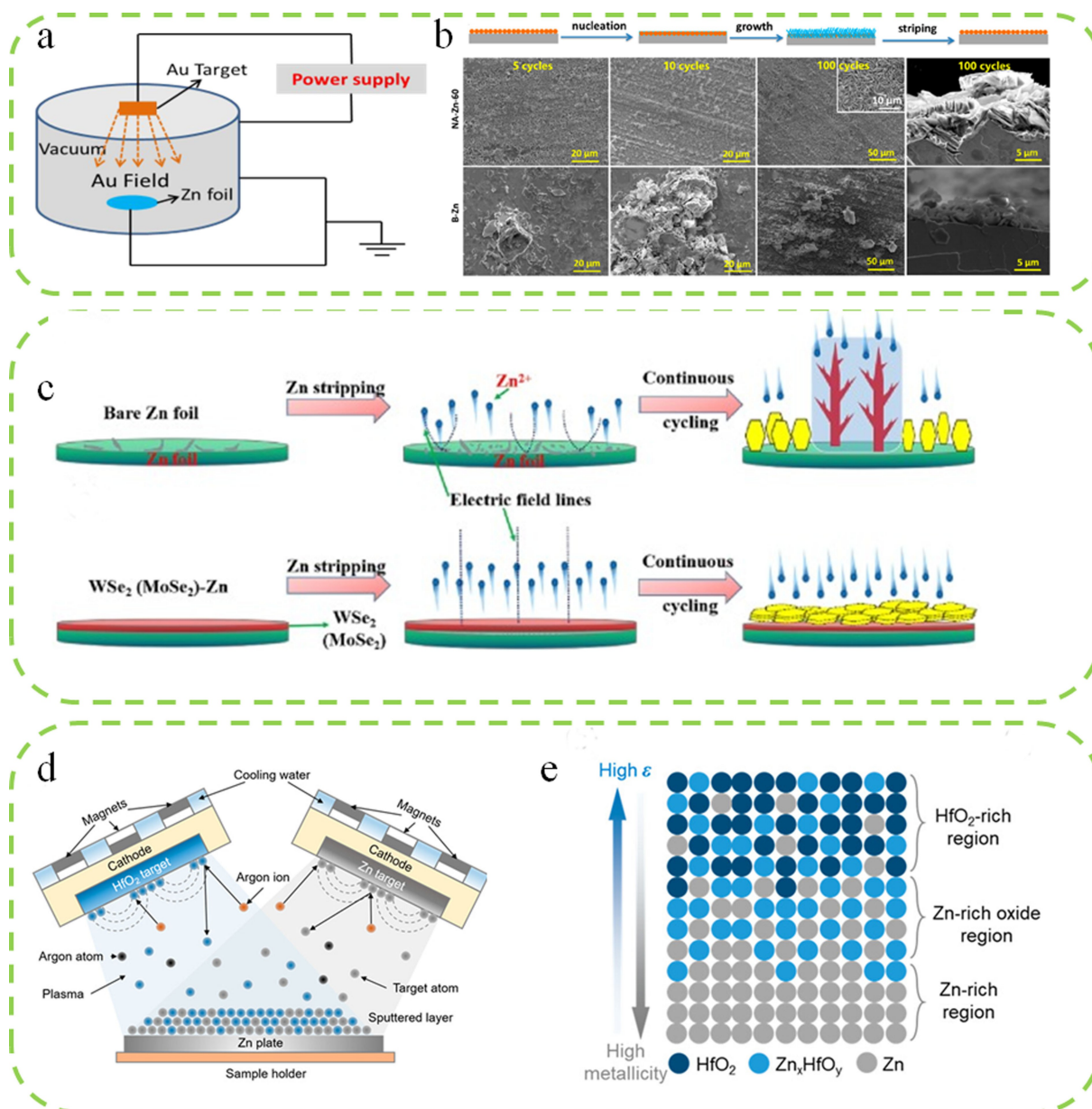


**Figure 6.** a) Preparation of Au nanoparticle decorated Zn foils (NA-Zn anodes). b) Schematic illustration of Zn plating/stripping on NA-Zn-60 and typical SEM images of NA-Zn-60 and bare Zn after different Zn plating/stripping cycles at a current density of  $0.25 \text{ mA cm}^{-2}$  and an area capacity of  $0.05 \text{ mAh cm}^{-2}$ . Reproduced from ref. [66] Copyright (2019), with permission from American Chemical Society. c) Schematic illustrations of morphology evolution for bare Zn foil and WSe<sub>2</sub>-Zn (MoSe<sub>2</sub>-Zn) during Zn stripping/plating cycling. Reproduced from ref. [44c] Copyright (2023), with permission from Elsevier. d) Illustration of the magnetron cosputtering process on Zn metal. e) Illustration of the composition distribution inside the Zn-GZH. Reproduced from ref. [67] Copyright (2023), with permission from American Chemical Society.

CVD is a prevailing strategy for coating thin films on the surface of the substrate, where the material vapor reacts with the substrate within a specific atmosphere.<sup>[68]</sup> Typically, the CVD process comprises several key stages. The reactant gases are first introduced into the reactor, followed by adsorption and diffusion onto the surface of the substrate, which lead to chemical reactions occurring at the solid/gas interface, ultimately resulting in the deposition of films.<sup>[43a]</sup> Based on this method, ZnSe coating was built on the surface of Zn foil.<sup>[69]</sup> During the process, the Se powder and Zn foil were placed in the upstream and downstream in a tube furnace, respectively,

where the Se powder was evaporated and subsequently reacted with the Zn foil to form a layer of ZnSe (Figure 7a). The recognizable X-ray diffraction (XRD) patterns, combined with mapping, confirmed the successful formation of the ZnSe layer (Figure 7b and c). Surface wettability was a key parameter for facilitating reversible Zn stripping/plating. As shown in Figure 7(d), the bare Zn foil displayed a contact angle of  $82^\circ$ , while the ZnSe@Zn sharply declined to  $14^\circ$ , indicating that the introduction of ZnSe enhanced surface wettability, thereby promoting the transport of  $\text{Zn}^{2+}$ . As shown in Figure 7(e), the Zn foil and NaH<sub>2</sub>PO<sub>4</sub> powder reacted at  $415^\circ\text{C}$  for 4 h under

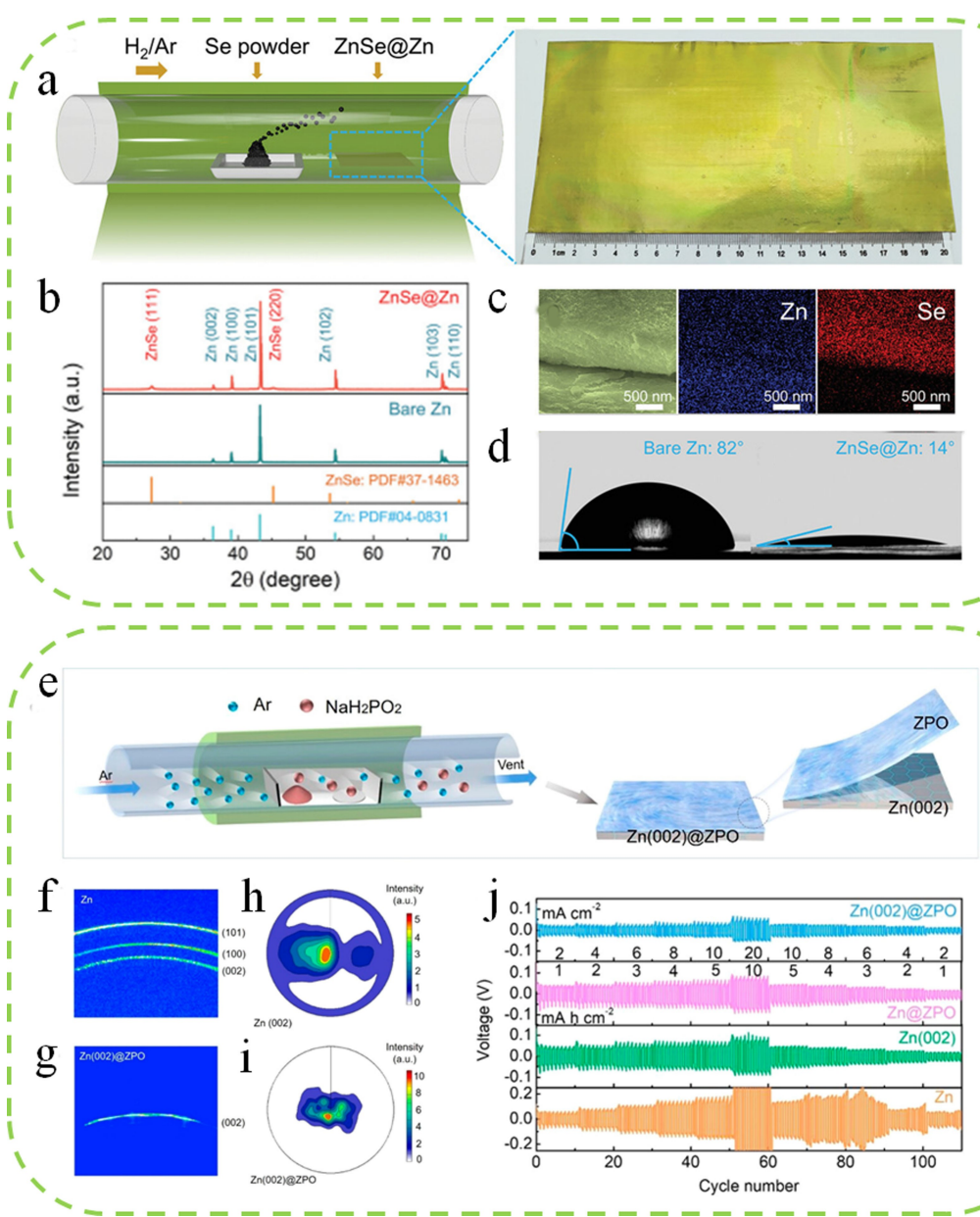


**Figure 7.** a) Schematic illustration of CVD growth of uniform ZnSe overlayer on Zn foil and photograph showing a ZnSe@Zn product. b) XRD patterns of bare Zn and obtained ZnSe@Zn. c) Side-view SEM and elemental maps of ZnSe@Zn. d) Digital photo showing the contact angle values of ZnSO<sub>4</sub> electrolyte on bare Zn and 0.75 μm-thick ZnSe@Zn. Reproduced from ref. [69] Copyright (2021), with permission from Wiley-VCH. e) Fabrication process of Zn(002)@ZPO. f) 2D XRD patterns of bare Zn and g) Zn(002)@ZPO and pole figures of h) Zn(002) on bare Zn and i) Zn(002)@ZPO. j) Rate performance of the symmetric cells. Reproduced from ref. [70] Copyright (2023), with permission from American Chemical Society.

50 sccm Ar.<sup>[70]</sup> After the reaction, an amorphous layer of ZPO with (002) plane was successfully coated on the Zn foil (Zn(002)@ZPO). The preferential orientation of Zn foil was confirmed by two-dimensional (2D) XRD patterns and X-ray diffraction pole figures. The bare Zn foil exhibited three Debye rings, indicative of its polycrystalline and randomly oriented nature, while the Zn(002)@ZPO displayed only one ring, illustrating the transition to preferential orientation (Figure 7f and g). The pole figures revealed that Zn(002) was widely distributed on the bare Zn foil but concentrated on Zn(002)-@ZPO, confirming the preferential surface exposure of Zn(002) in the case of Zn(002)@ZPO (Figure 7h and i). It was noted that

Zn(002)@ZPO effectively lowered diffusion energy barriers, suppressed side reactions, and facilitated even Zn<sup>2+</sup> deposition. Owing to the synergistic effects of ZPO and Zn(002), symmetric cells based on Zn(002)@ZPO worked stably for over 500 h under a DOD≈68 %. The superior electrochemical performance of the Zn(002)@ZPO was further identified by the rate performance, indicating enhanced reaction kinetics (Figure 7j).

In a word, the vapor deposition provides a novel way for the uniform deposition of coating layers without engaging in liquid-phase reactions, which is suitable for a wide range of materials, including metal and non-metallic materials. Moreover, the in-situ layers possess favorable conformity and strong

adhesion to the surface of Zn anode. Nevertheless, the high cost of the vapor deposition restricts the large-scale application.

### 3.6. Atomic/molecule layer deposition

The atomic layer deposition (ALD) is a crucial technique to construct a thin layer, where the gaseous reactants are sequentially pulsed into the reaction chamber and the chemical reactions occur on the surface of the target substrate, ultimately resulting in the formation of a film.<sup>[71]</sup> By-products and residual precursors can be effectively eliminated by sweeping with inert gas or evacuation.<sup>[71]</sup> ALD provides an advanced method to prepare conformal and uniform layers with controllable thickness and high quality at the atomic scale.<sup>[72]</sup> For example, an Al<sub>2</sub>O<sub>3</sub>-coated Zn anode was prepared by ALD.<sup>[73]</sup> In the synthesis process, Al(CH<sub>3</sub>)<sub>3</sub> and H<sub>2</sub>O were alternately introduced into the reactor with Ar purging to form an Al<sub>2</sub>O<sub>3</sub> layer on the surface of the Zn anode (Al<sub>2</sub>O<sub>3</sub>@Zn) (Figure 8a). The thickness of the coating had a significant effect on the cycling stability, whose

thickness was controlled by the number of ALD cycles. The optimized 60Al<sub>2</sub>O<sub>3</sub>@Zn exhibited stable cycling beyond 100 h and demonstrated the lowest hysteresis voltage, suggesting that the optimized Al<sub>2</sub>O<sub>3</sub> layer minimized cell polarization and inhibited dendrite formation (Figure 8b). Furthermore, the assembled AVNF//60Al<sub>2</sub>O<sub>3</sub>@Zn exhibited superior electrochemical performances as well. In light of the versatility of ALD, an ultrathin ZrO<sub>2</sub> coating layer was also prepared by ALD (Zn@ZrO<sub>2</sub>), resulting in excellent cycling life and high-performance Zn–MnO<sub>2</sub> batteries.<sup>[71]</sup> In this process, tetrakis (dimethylamino) zirconium (TDMAZr) and H<sub>2</sub>O were pulsed into the vacuum chamber, and repeated above cycles to achieve ultrathin ZrO<sub>2</sub> layers (Figure 8c). The as-obtained Zn@ZrO<sub>2</sub> effectively regulated even Zn deposition, as confirmed by 3D laser confocal microscope and SEM. As shown in Figure 8(d–g), the pristine surface of the bare Zn and ZrO<sub>2</sub>@Zn displayed similar levels of roughness, but the ZrO<sub>2</sub>@Zn demonstrated a flatter film than bare Zn after 50 cycles. From the SEM images, it could be observed that the surface was covered by by-products on the bare Zn, while the surface of the ZrO<sub>2</sub>@Zn remained

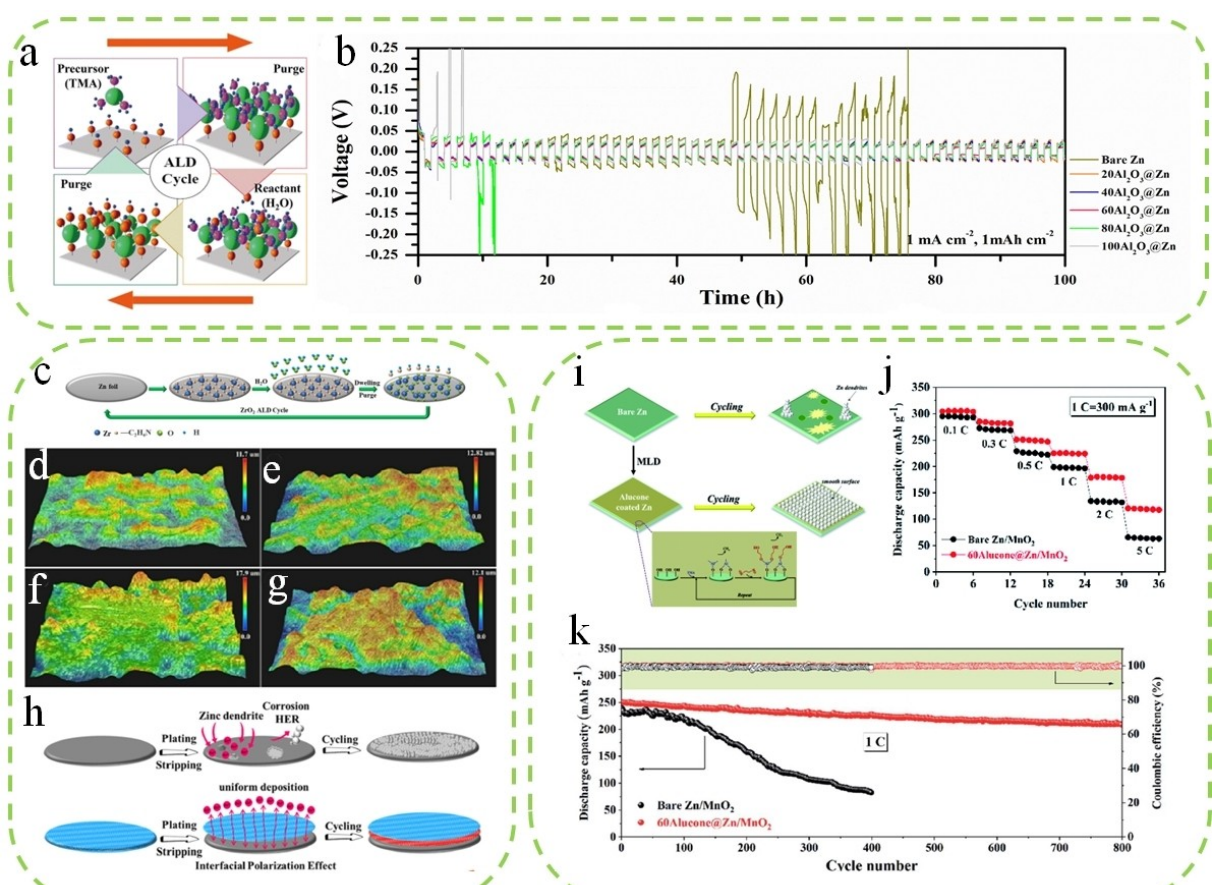


**Figure 8.** a) A scheme for the deposition of Al<sub>2</sub>O<sub>3</sub> formed by the reaction of Al(CH<sub>3</sub>)<sub>3</sub> and H<sub>2</sub>O in an ALD cycle. b) Zn-Zn symmetric cell at 1 mA cm<sup>-2</sup>. Reproduced from ref. [73] Copyright (2023), with permission from The Royal Society of Chemistry. c) Schematic illustration of the fabrication process of the inorganic ZrO<sub>2</sub> coating on Zn metal anodes by ALD. 3D confocal microscope image of d) bare Zn and e) 40 nm ZrO<sub>2</sub>@Zn, and f) bare Zn and g) 40 nm ZrO<sub>2</sub>@Zn after 50 cycle tests at 1 mA cm<sup>-2</sup> with a capacity of 1 mAh cm<sup>-2</sup>. h) Schematic illustration of the Zn plating process on the bare Zn and the ZrO<sub>2</sub>@Zn. Reproduced from ref. [71] Copyright (2022), with permission from Elsevier. i) Schematic illustration showing the effect of inorganic-organic MLD alucone coating on Zn metal anodes when cycling. j) Rate capability of bare Zn/MnO<sub>2</sub> and 60alucone@Zn/MnO<sub>2</sub> full cells ranging from 0.1 to 5 C. k) Long-term cycling stability of bare Zn/MnO<sub>2</sub> and 60alucone@Zn/MnO<sub>2</sub> full cells at a current density of 1 C. Reproduced from ref. [74] Copyright (2020), with permission from The Royal Society of Chemistry.

homogeneous and dense, effectively inhibiting Zn dendrite growth. The  $\text{ZrO}_2$  coating layer not only avoided direct contact between the Zn anode and electrolyte for suppressing side reactions, but also boosted the desolvation process of  $\text{Zn}^{2+}$  for fast ion kinetics (Figure 8h).

Numerous materials can be applied to modify the surface by ALD, such as sulfides, oxides, nitrides, and so on, which can significantly alleviate the problems of Zn anodes, but this method is only applicable to the preparation of inorganic coatings.<sup>[20]</sup> Therefore, molecule layer deposition (MLD) acted as a sister technique is emerging for constructing organic-inorganic hybrid films at the molecular level. As shown in Figure 8(i), a novel ultrathin protective layer was successfully prepared by MLD.<sup>[74]</sup> Consequently, the optimized Zn anode with 60 MLD cycles (60alucone@Zn) demonstrated an extended cycling life (over 780 h) at  $3 \text{ mA cm}^{-2}$  and a reduced overpotential (about 84.3 mV), which was due to the fact that the coating could effectively suppress dendrite growth and guide uniform Zn deposition. Moreover, the as-assembled  $\text{MnO}_2/60\text{Alucone@Zn}$  delivered superior cycling and rate performance compared to the bare  $\text{MnO}_2/\text{Zn}$  (Figure 8j and k).

In summary, ALD and MLD demonstrate exceptional reproducibility for constructing high-quality deposition layers at the atomic and molecular scale, whose thickness can be precisely controlled by cyclic number. However, the cost of the two technologies is expensive and the preparation is relatively complicated. Therefore, these methods have little prospect for large-scale application at present.

### 3.7. 3D printing

3D printing is an additive manufacturing technology. Based on digital models, the adhesive materials are printed with a 3D printer to create complex shapes via layer by layer.<sup>[55]</sup> And the printing process is controlled by the computer, which ensures precise construction of unique 3D structures on the substrate.<sup>[51]</sup> The printing process mainly includes following fundamental stages. A 3D model is first obtained by computer software, followed by the preparation of a homogenous ink transferred to a syringe. Subsequently, the designed model is printed to the substrate via a 3D printer. Finally, the printed product is obtained through solvent evaporation. Recently, Liu et al. reported a uniformly distributed  $\text{g-C}_3\text{N}_4$  layer with a unique 3D structure on the surface of Zn foil as a zincophilic interface to stabilize the Zn anode and suppress the Zn dendrite growth (Figure 9a).<sup>[75]</sup> The  $\text{g-C}_3\text{N}_4$  with abundant N species was conducive to binding with  $\text{Zn}^{2+}$ , which was further supported by DFT calculations (Figure 9b–e). The binding energy of  $\text{g-C}_3\text{N}_4$  with  $\text{Zn}^{2+}$  ( $-1.24\text{ eV}$ ) was significantly higher than the bare Zn ( $-0.68\text{ eV}$ ), indicating that  $\text{g-C}_3\text{N}_4$  improved the binding strength of  $\text{Zn}^{2+}$ . A deeper understanding of the enhanced binding energy was elucidated through charge density analysis. The high electronegativity of N in  $\text{g-C}_3\text{N}_4$  resulted in a stronger coulomb interaction with  $\text{Zn}^{2+}$ , culminating in a relatively stable structure. Therefore,  $\text{g-C}_3\text{N}_4$  could afford more zincophilic sites that guided the uniform deposition of  $\text{Zn}^{2+}$ , facilitating a reversible Zn plating/stripping process. Meanwhile, the coating

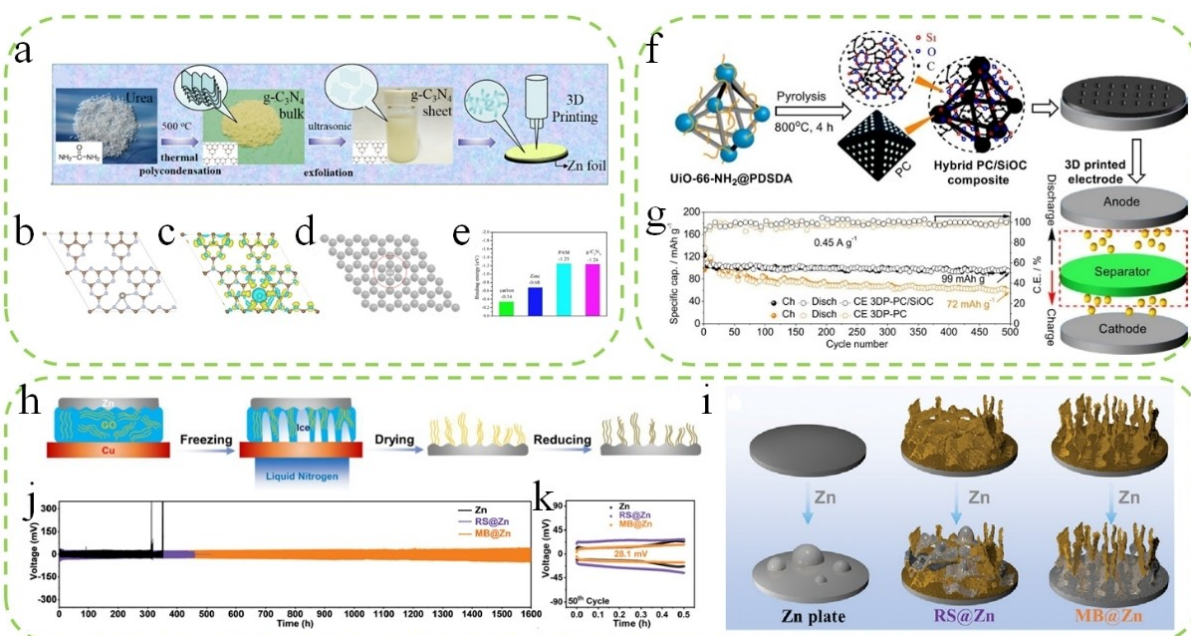


**Figure 9.** a) Schematic illustration of the fabrication process and application of thin  $\text{g-C}_3\text{N}_4$  nanosheets. b) Crystal models for calculating the binding energy of a  $\text{Zn}^{2+}$  adsorbed on  $\text{g-C}_3\text{N}_4$  and c) the corresponding charge density difference (yellow and light blue areas represent positive and negative charge differences, respectively). d) Crystal models for calculating the binding energy of a  $\text{Zn}^{2+}$  adsorbed on Zn. e) Binding energy of a  $\text{Zn}^{2+}$  with different substrates. Reproduced from ref. [75] Copyright (2021), with permission from Elsevier. f) Schematic illustration of the hybrid PC/SiOC composite preparation. g) Comparison of cycle performance of 3DP-PC/SiOC@Zn and 3DP-PC@Zn. Reproduced from ref. [76] Copyright (2022), with permission from Elsevier. h) Schematic illustration of the preparation of MB@Zn. i) Schematic of dendritic Zn formation on Zn, RS@Zn, and MB@Zn during Zn deposition. j) Long-term galvanostatic cycling performance and k) the corresponding 50<sup>th</sup> cycle of symmetrical cells from designed electrodes at  $0.2 \text{ mA cm}^{-2}$  within charging/discharging time of 0.5 h. Reproduced from ref. [78] Copyright (2022), with permission from Wiley-VCH.

with unique 3D architecture established channels for ion and electron transport. Consequently, symmetric cells based on Zn/C<sub>3</sub>N<sub>4</sub> displayed an extended cyclic lifespan. Meanwhile, the electrochemical performances of Zn//C<sub>3</sub>N<sub>4</sub>//MnO<sub>2</sub> and Zn/C<sub>3</sub>N<sub>4</sub>/AC systems were enhanced as well. It is worth noting that hybrid composites can also be utilized as coatings by a 3D printer. For instance, Idrees et al. constructed a hybrid composite as a protective layer to modify Zn foil.<sup>[76]</sup> The hybrid UiO-66-NH<sub>2</sub>/poly[(silylene)diacetylenes] (UiO-66-NH<sub>2</sub>/PDSDA) composite was prepared by UiO-66-NH<sub>2</sub> coordinated with PDSDA through a polymerization, and then UiO-66-NH<sub>2</sub>/PDSDA was calcined to obtain hybrid silicon oxycarbide coated porous carbon (PC/SiOC). Finally, 3D printed PC/SiOC@Zn (3DP-PC/SiOC@Zn) was achieved by 3D printing technology for assembling the full cells (Figure 9f). The optimized 3DP-PC/SiOC@Zn afforded tunable spaces for Zn<sup>2+</sup> migration, ensuring uniform Zn deposition and controlling dendrite growth, which delivered exceptional electrochemical performances (Figure 9g).

In summary, 3D printing, as an advanced technology, can construct coatings with complex structures. The preparation procedure is simple and high-repeatability, and the model establishment and printing process are mainly controlled by computer. With the unique 3D structures, the as-prepared coating layers can effectively promote ion migration. Unfortunately, the cost of this method is relatively high, and the range of materials suitable for 3D printing is limited, which currently restricts its widespread application at a larger scale.

### 3.8. Vacuum freezing drying method

Vacuum freeze-drying technology, also known as freeze-drying technology, the fundamental principle is sublimation, namely the transfer from a solid into a gas under vacuum conditions.<sup>[77]</sup> The process mainly includes three steps. Initially, pre-freezing lowers the temperature below the material's eutectic point to induce freezing. Then the ice was sublimated to extract water from the material. Finally, secondary drying is conducted to eliminate the residual moisture. Recently, Huang et al. successfully prepared carbon-based oxygen-containing microbrushes on Zn foil (MB@Zn) by freeze-drying technology (Figure 9h).<sup>[78]</sup> These oxygen-containing functional groups in the microbrushes have a strong affinity for Zn<sup>2+</sup>, effectively guiding Zn<sup>2+</sup> deposition and inhibiting side reactions. Detailed comparisons revealed that MB@Zn demonstrated superior Zn plating/stripping properties than those of bare Zn foil and covered with randomly arranged sheets (RS@Zn), evidencing the synergistic effects of chemical and structural design of the zincophilic alignment (Figure 9i). Consequently, MB@Zn delivered significantly enhanced electrochemical performances, including a small voltage hysteresis (28.1 mV) and a long lifespan (> 1600 h) (Figure 9j and k).

In summary, freeze-drying technology can prevent the intrinsic properties of the materials from denaturation, shrinkage or toughening during the drying process. Therefore, this method establishes a stable, loose and porous artificial coating

for ion migration, but the process is time-consuming, limiting large-scale applications.

### 3.9. Others

In addition to the methods mentioned above, there are some other methods for constructing coatings, such as pencil drawing,<sup>[79]</sup> spray-coating method,<sup>[80]</sup> pasting<sup>[81]</sup> and so on. These methods are simple and flexible, yet their scalability to large applications remains challenging. The electrochemical performances of Zn anodes with different interfacial engineering strategies are presented in Table 1. In summary, various methods have unique features in constructing coating layers, and therefore it is vital to select an appropriate strategy to modify the Zn anodes. We have summarized the pros and cons of the proposed methods in the Table 2.

## 4. Electrolyte Optimization

In addition to surface coatings, optimization of electrolyte is a crucial aspect of interface engineering to alleviate cross talk. Three frequently adopted approaches including the introduction of additives into electrolyte, water-in-salt electrolyte (WIS), and quasi-solid gel electrolytes engineering can purposefully inhibit the undesirable migration of certain species and therefore efficiently suppress electrode cross talk.<sup>[18a,46]</sup> Electrolyte additives have demonstrated success in solving the above problems. For instance, a pH buffer solution consisting of N-containing organic molecules, namely pyridine and imidazole, was practical for dendrite-free and shuttle-free, achieving long-cycle Zn-I<sub>2</sub> batteries. Specifically, addition of imidazole and pyridine regulated changes in pH within the electrolyte, suppressing HER and corrosion through the formation/release of N-H bonds. Moreover, pyridine and imidazole preferentially adsorbed on the surface of Zn anodes, suppressing dendritic growth and facilitating the even deposition of Zn. In addition, pyridine additive reduced conversion barriers for I<sub>2</sub>/I<sup>-</sup> and inhibited the generation of intermediate (I<sub>3</sub><sup>-</sup>), boosting reversibility and stability of Zn-I<sub>2</sub> batteries.<sup>[99]</sup> Water-in-salt electrolyte plays a crucial role in achieving long cycling life Zn-I<sub>2</sub> batteries. Ji et al. explored the Zn-I<sub>2</sub> batteries utilizing the ZnCl<sub>2</sub>/KI water-in-salt (WIS) electrolyte. This WIS electrolyte, featured with a high salt concentration, effectively reduced the presence of free water, consequently mitigating undesirable side reactions on the Zn anode. Additionally, the iodine in the electrolyte preferentially integrated into the solvation layer of Zn<sup>2+</sup> rather than forming I<sub>3</sub><sup>-</sup> through coordination with I<sub>2</sub>, thereby inhibiting the shuttle effect. As a result, the batteries delivered an improved CE of 95%, a superior rate performance and an excellent cycling stability.<sup>[100]</sup> Apart from electrolytic additives and WIS electrolytes, quasi-solid gel electrolytes have demonstrated great potential in limiting cross talk. Recently, Sonigara et al. integrated an amphiphilic block copolymer (F77, PEO<sub>53</sub>-PPO<sub>34</sub>-PEO<sub>53</sub>) to form solid gel electrolyte. In particular, water molecular was trapped in the cross-linked network of F77 to

**Table 1.** Summary of different strategies for interfacial engineering of Zn anodes.

| Artificial interphase            | Processing method          | Electrolyte                               | Current ( $\text{mA cm}^{-2}$ ) @ capacity ( $\text{mAh cm}^{-2}$ ) | Lifespan (h) | Refs. |
|----------------------------------|----------------------------|---|---|--------------|-------|
| UO                               | Doctor blading             | 2 M $\text{ZnSO}_4$                       | 1@1   | 1600         | [82]  |
| Fullerene $C_{60}$ nanomaterials | Doctor blading             | 2 M $\text{ZnSO}_4$                       | 0.25@0.25   | 3800         | [83]  |
| HZBL                             | Spin-coating               | 2 M $\text{ZnSO}_4$                       | 1@1   | 2500         | [84]  |
| STO                              | Spin-coating               | 2 M $\text{ZnSO}_4$                       | 0.5@0.5   | 4000         | [85]  |
| MOF-CeO <sub>2</sub>             | Spin-coating               | 3 M $\text{Zn}(\text{TfO})_2$             | 3@1   | 3200         | [86]  |
| NOC                              | CVD                        | 2 M $\text{ZnSO}_4$                       | 1@1   | 3040         | [87]  |
| PAAZn                            | CSD                        | 2 M $\text{ZnSO}_4$                       | 1@1   | 2850         | [40c] |
| PANI                             | CSD                        | 2 M $\text{ZnSO}_4$                       | 3@1.5   | 500          | [16b] |
| ZnP                              | Electrochemical deposition | 2 M $\text{ZnSO}_4$                       | 2@0.5   | 3300         | [63]  |
| ZnF <sub>2</sub>                 | Electrochemical deposition | 2 M $\text{ZnSO}_4$                       | 1@1   | 800          | [62]  |
| BN                               | PVD                        | 2 M $\text{ZnSO}_4$                       | 1@1   | 3000         | [88]  |
| ZnTe                             | PVD                        | 2 M $\text{ZnSO}_4$                       | 1@1   | 5000         | [89]  |
| SnO <sub>2</sub>                 | ALD                        | 2 M $\text{ZnSO}_4$                       | 0.25@0.05   | 300          | [90]  |
| ZrO <sub>2</sub>                 | ALD                        | 2 M $\text{ZnSO}_4$                       | 1@0.5   | 1750         | [71]  |
| 60alucone                        | MLD                        | 3 M $\text{Zn}(\text{SO}_3\text{CF}_3)_2$ | 3@1   | 780          | [74]  |
| Graphite                         | Pencil drawing             | 2 M $\text{ZnSO}_4$                       | 0.1@0.1   | 200          | [79]  |
| FP                               | Pasting                    | 2 M $\text{ZnSO}_4$                       | 1@1   | 480          | [81]  |
| MNC                              | spray-coating              | 1 M $\text{ZnSO}_4$                       | 10@1  | 1200         | [80]  |
| PVA@SR                           | Vacuum freeze-drying       | 3 M $\text{ZnSO}_4$                       | 2@2   | 2000         | [77]  |
| P-0.5%MXene                      | 3D printing                | 2 M $\text{ZnSO}_4$                       | 1@1   | 4200         | [91]  |

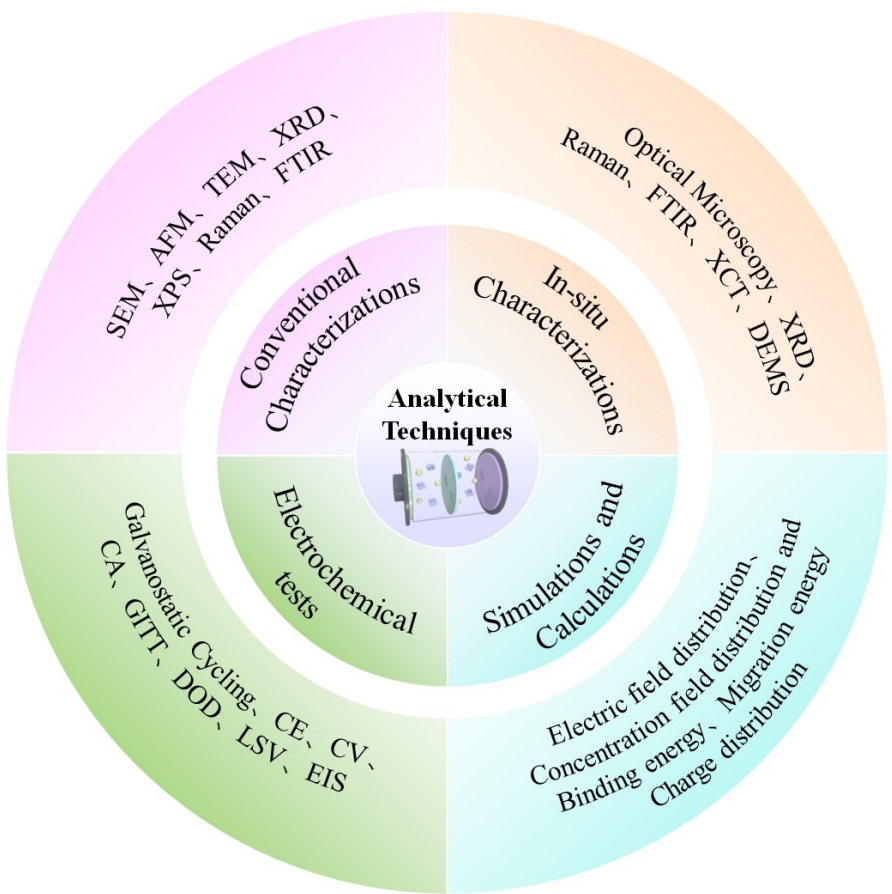
**Table 2.** Comparison of different operation methods and processes of modified zinc anode.

| Method                           | Advantages   | Drawbacks  | Refs.         |
|----------------------------------|--|--|---------------|
| Doctor blading                   | <ul style="list-style-type: none"> <li>Simple workflow</li> <li>Low cost</li> <li>Suitable for most materials on the market</li> </ul> | <ul style="list-style-type: none"> <li>Toxicity</li> <li>Thick coating</li> </ul>  | [92]          |
| Spin-coating                     | <ul style="list-style-type: none"> <li>Controllable thickness</li> <li>High repeatability</li> </ul>                                   | <ul style="list-style-type: none"> <li>Toxicity</li> <li>Unfavorable for large-scale manufacturing</li> </ul>                    | [93]          |
| Chemical solution deposition     | <ul style="list-style-type: none"> <li>Affordable cost</li> <li>Simple engineering workflow</li> <li>Strong adhesion</li> </ul>        | <ul style="list-style-type: none"> <li>Uncontrollable thickness</li> <li>Poor repeatability</li> </ul>                           | [16b, 87, 94] |
| Electrochemical deposition       | <ul style="list-style-type: none"> <li>Simple preparation</li> <li>Swift optimizations</li> </ul>                                      | <ul style="list-style-type: none"> <li>Limited materials</li> <li>Unfavorable for precise growth control</li> </ul>              | [95]          |
| Vapor deposition                 | <ul style="list-style-type: none"> <li>Controllable thickness and uniformity</li> <li>High repeatability</li> </ul>                    | <ul style="list-style-type: none"> <li>High cost</li> <li>Toxicity</li> <li>Unfavorable for large-scale manufacturing</li> </ul> | [88, 89, 96]  |
| Atomic/molecule layer deposition | <ul style="list-style-type: none"> <li>Precise control of thickness</li> </ul>   | <ul style="list-style-type: none"> <li>High cost</li> <li>Complicated workflow</li> </ul>  | [71, 74, 97]  |
| 3D printing                      | <ul style="list-style-type: none"> <li>Construction of unique 3D architectures</li> <li>Superior repeatability</li> </ul>              | <ul style="list-style-type: none"> <li>High cost</li> <li>Limited materials</li> </ul>   | [75, 76]      |
| Vacuum freezing drying           | <ul style="list-style-type: none"> <li>Establishing a stable and porous artificial coating</li> </ul>                                  | <ul style="list-style-type: none"> <li>Time-consuming operation</li> <li>Unfavorable for large-scale manufacturing</li> </ul>    | [77, 98]      |

avoid the hydrogen evolution and corrosion of Zn anode. Moreover, the microcrystalline structure can effectively block shuttle iodine species by ion selective hydrophilic/hydrophobic channels. Consequently, the assembled Zn-I<sub>2</sub> batteries presented high electrochemical performances.<sup>[101]</sup> Therefore, the rational design of electrolytes is conducive to inhibiting cross talk.

## 5. Analytical Techniques

A large of works have elucidated the vital roles of coating layers in stabilizing the Zn anode. To achieve a comprehensive understanding of the working mechanism of coating layers, it is imperative to develop advanced characterizations with theoretical calculations and simulations, which provide fundamental guidance for layer design (Scheme 2). The applications of



Scheme 2. The reported analytical techniques of interfacial engineering in ZIBs.

advanced characterization techniques for the study of ZIBs will be summarized from the following critical aspects: (1) conventional techniques; (2) electrochemical tests; (3) in-situ characterizations; (4) simulations and calculations.

To qualitatively and quantitatively assess the effectiveness of strategies, various analytical methods are adopted to understand the properties of coating layers. Some conventional techniques can provide preliminary information.<sup>[102]</sup> To assess the extent of corrosion of Zn anodes, the by-products ( $Zn_4SO_4(OH)_6 \cdot xH_2O$ ) are examined by XRD and SEM. XRD, relying on constructive interference of monochromatic X-rays and crystalline samples, produces distinctive diffraction patterns that provide insights into the crystalline phases of materials and lattice parameters at the unit cell level. This technique holds significance in studying the electrochemical reactions of electrode materials during discharge and charge processes, allowing detection of structural changes and phase transitions. For example, the byproducts ( $Zn_4SO_4(OH)_6 \cdot xH_2O$ ) were often detected after the cycling on the bare Zn anode, whereas the modified Zn anode delivered no extra by-product peaks.<sup>[103]</sup> Moreover, a layer of loose by-products on the surface could be observed by SEM. Coupled with energy dispersive X-ray spectroscopy (EDS) mapping images, it further verified the formation of by-products on the surface of Zn anodes, confirming the inhibition of side reactions by interphase

modifications.<sup>[103]</sup> Raman spectroscopy and Fourier transform infrared (FTIR) offer complementary information on structure and composition. Recently, introduction of sulfolane (SL) into the electrolyte improved Zn anode reversibility, as evidenced by FTIR and Raman analyses.<sup>[104]</sup> The O–H stretching vibration in FTIR spectrum shifted to higher wavenumbers, indicating the additional SL destroyed the interaction between  $Zn^{2+}$  and water molecules, effectively alleviating the severe water decomposition. In addition, the Raman further analyzed the  $v(SO_4^{2-})$  in detail. The  $v(SO_4^{2-})$  band exhibited 62% of separated ion pair (SSIP) in SL/ $ZnSO_4$ , which was higher than that of  $ZnSO_4$  solution (49%), indicating that  $SO_4^{2-}$  had difficulty in entering the solvation structure of  $Zn^{2+}$  in the SL/ $ZnSO_4$  electrolyte, inhibiting the formation of by-products (Figure 10a). Atomic force microscopy (AFM), a versatile scanning probe microscopy technique, offers qualitative and quantitative insights into material characteristics, including morphology and roughness. Coupled with 3D laser confocal scanning microscope (LCSM), it can be further used to measure the morphology in a 3D mode. For instance, a multifunctional fluorapatite ( $Ca_5(PO_4)_3F$ ) aerogel (FAG) interface layer on the Zn anode was prepared. AFM and LCSM clearly demonstrated a smoother surface of cycled FAG@Zn than that of bare Zn, confirming the suppressed side reactions and dendrite growth (Figure 10b).<sup>[92a]</sup> XPS analysis serves as an effective tool for evaluating surface chemical

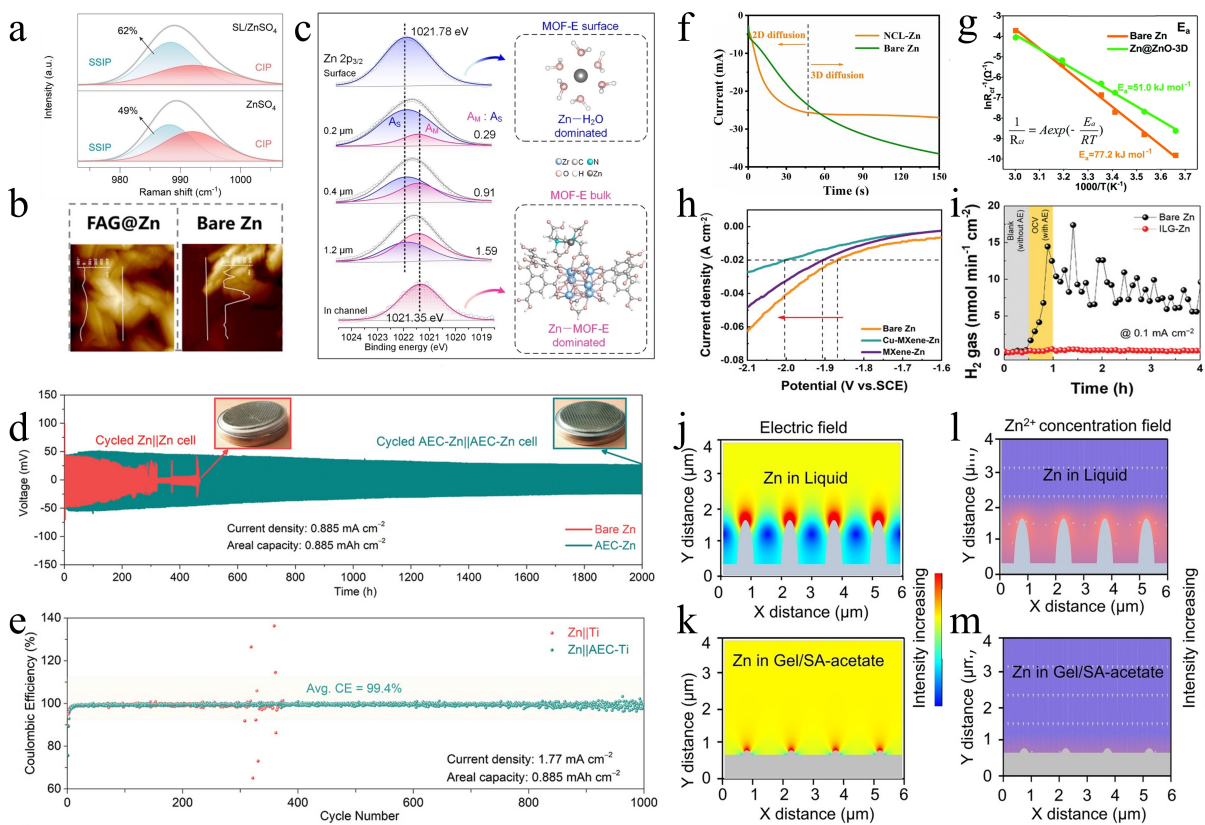


**Figure 10.** a) The Raman spectra of pure  $\text{ZnSO}_4$  and SL/ $\text{ZnSO}_4$  electrolytes. Reproduced from ref. [104] Copyright (2023), with permission from Elsevier. b) AFM images of the different anodes after 50 cycles. Reproduced from ref. [92a] Copyright (2023), with permission from American Chemical Society. c) XPS analysis with depth profiling of the cycled MOF-E@Cu at  $1 \text{ mA cm}^{-2}$  with  $0.5 \text{ mA cm}^{-2}$ . Reproduced from ref. [105] Copyright (2023), with permission from Wiley-VCH. d) Long-term cycling performance in symmetrical cells with a current density of  $0.885 \text{ mA cm}^{-2}$  with the inset showing the photos of the cycled cells. e) CE of Zn plating/stripping at a current density of  $1.77 \text{ mA cm}^{-2}$  with an ending charging voltage of  $0.2 \text{ V}$ . Reproduced from ref. [108] Copyright (2021), with permission from Wiley-VCH. f) CAs of NCL-Zn and bare Zn anodes. Reproduced from ref. [109] Copyright (2023), with permission from Elsevier. g) Arrhenius curves and comparison of activation energies of  $\text{Zn@ZnO-3D}$  and bare Zn. Reproduced from ref. [22d] Copyright (2020), with permission from the Royal Society of Chemistry. h) LSV curves of bare Zn, MXene-Zn, and Cu-MXene-Zn. Reproduced from ref. [92b] Copyright (2023), with permission from Wiley-VCH. i)  $\text{H}_2$  gas signal of the ILG-Zn (vs bare Zn) as a function of time, which was obtained by in situ DEMS analysis at a current density of  $0.1 \text{ mA cm}^{-2}$ . Reproduced from ref. [114] Copyright (2021), with permission from Wiley-VCH. Electric field of Zn anodes in j) pure  $\text{ZnSO}_4$  and k) Gel/SA-acetate.  $\text{Zn}^{2+}$  flux distributions near Zn anode in l) pure  $\text{ZnSO}_4$  and m) Gel/SA-acetate. Reproduced from ref. [117] Copyright (2023), with permission from Wiley-VCH.

environments, encompassing the valence state of elements and their content. Zhang et al proposed ethylenediaminetetraacetic acid (EDTA) grafted metal organic framework (MOF-E) as an interphase for Zn anodes.<sup>[105]</sup> XPS tests revealed the evolutions of  $\text{Zn}^{2+}$  solvation structure in the MOF-E layer. The high-resolution Zn 2p spectrum could be divided into Zn-EDTA and Zn-OH<sub>2</sub>. As the etching time prolonged, the ratio of Zn-EDTA to Zn-OH<sub>2</sub> was increasing, suggesting the MOF-E layer facilitated the desolvation process (Figure 10c). From these results, a series of basic information can be obtained, which is conducive to illustrating the possible reaction mechanisms during the electrochemical process.

Electrochemical characterizations play a crucial role in directly evaluating the electrochemical properties of materials and the effectiveness of strategies.<sup>[53,106]</sup> Various electrochemical tests are usually employed to investigate Zn anodes, including cyclic voltammetry (CV), galvanostatic cycling test, linear sweep voltammetry (LSV), chronoamperometry (CA), electrochemical impedance spectroscopy (EIS), CE, DOD, and so on. Typically, CV tracks the current as a function of voltage, providing current-

voltage profiles that yield valuable insights into electrochemical reactions, cycling reversibility and electrochemical windows. Moreover, differences in peak position and ratio can be used to evaluate the degree of electrode reversibility and potential side reactions. Lu et al. performed CV curves to investigate the effects of arginine (Arg) on Zn plating/stripping.<sup>[107]</sup> The overpotential in  $\text{ZnSO}_4$  with Arg electrolyte was larger than that of bare  $\text{ZnSO}_4$  electrolyte, increased by nearly  $30 \text{ mV}$ , which was favorable nucleation of fine and dense grains. Galvanostatic cycling tests are widely carried out for commercial and laboratory batteries, evaluating the effectiveness of strategies used in batteries, including the CE, the cycling life and the DOD. For example, Zhao et al. constructed an anti-corrosion elastic constraint (AEC) as an artificial protective layer to induce uniform deposition of Zn.<sup>[108]</sup> The stability of the Zn anode was assessed by the galvanostatic cycling of symmetric cells. The coated Zn cell displayed a lifespan of over  $2000 \text{ h}$ , which was longer than that of bare Zn, indicating that the artificial protective layer could effectively suppress dendrites and side reactions (Figure 10d). More importantly, the AEC-Zn demon-

strated steady charge/discharge curves even under a DOD of 60%. In addition, the CE of Zn stripping/plating could be obtained by Zn||Ti asymmetric cells to test the reversibility of the Zn/Zn<sup>2+</sup> chemistry. The bare Zn||Ti cell exhibited obvious voltage fluctuation and low CE, whereas the Zn||AEC-Ti cell displayed a better cycle performance, with an average CE of 99.4%, contributing to reversible reactions (Figure 10e). The CA measurements are used to investigate the mechanism of Zn deposition, where the current as a function of time under a constant potential reflects the nucleation process and surface change. As shown in Figure 10(f), the bare Zn maintained steady over 150 s, corresponding to the long 2D diffusion process, whereas the nitrogen doped carbon network coated Zn anode significantly shortened to 47 s, indicating quickly achieved stable 3D diffusion, which was of importance to facilitate the uniform Zn deposition.<sup>[109]</sup> EIS is an electrochemical characterization to provide kinetic information. The activation energy ( $E_a$ ) can be calculated by fitting  $R_{ct}$  to assess the desolvation capability of Zn<sup>2+</sup>. Figure 10(g) displayed that the  $E_a$  of Zn anodes modified by a three-dimensional nanoporous ZnO architecture (51.0 kJ mol<sup>-1</sup>) was lower than that of bare Zn (77.2 kJ mol<sup>-1</sup>), evidencing the fast desolvation enabled by regulation of the solvation sheath in electric double layers.<sup>[22d]</sup> LSV can analyze the inhibition of H<sub>2</sub> evolution. Figure 10(h) presented the potential of HER on the bare Zn electrode was -1.86 V, while on the MXene modified Zn (MXene-Zn) and MXene with the modification of Cu coated Zn (Cu-MXene-Zn) electrodes were -1.90 and -2.00 V, respectively, suggesting that the protective layers effectively inhibited the HER.<sup>[92b]</sup> However, it is worth noting that these conventional characterizations are infeasible to real-time detect the changes of Zn anode.

The electrochemical processes of ZIBs are involved with sensitive and complicated interfacial chemistry. Therefore, in-situ techniques are particularly attractive as they enable real-time monitoring of structural, compositional and crystalline changes during electrochemical processes, which is significant for getting insights into underlying mechanisms and advancing practical applications of ZIBs. In-situ optical microscopy is a common tool for observing changes of the morphological structure in real time.<sup>[110]</sup> A serious dendrite growth could be observed in the bare Zn symmetric cell while the Zn anode with polyamide (PA) layer maintained a smooth surface, evidencing the effectiveness of the protective layer to suppress dendrite growth.<sup>[111]</sup> X-ray computed tomography (XCT) is a powerful imaging technique to directly visualize dendrite growth reconstructed in a 3D level.<sup>[112]</sup> Yufit et al utilized in-situ XCT for the first time to investigate the Zn anodes during the plating/stripping process. It could be clearly observed that dendrites continued to grow until they penetrated the separator and expanded in different directions to form a complex branch network on top during the Zn deposition, then the dendrites started to dissolve during the stripping process. This approach significantly promoted the understanding of Zn deposition/stripping behavior, providing insights into effective strategies.<sup>[25]</sup> During the Zn plating process, hydrogen evolution and Zn deposition are a competitive reaction. Differential electrochem-

ical mass spectrometry (DEMS) is a valid technique for in-situ detection of hydrogen evolution to analyze the electrolyte compatibility with Zn.<sup>[113]</sup> In contrast with the bare Zn, the H<sub>2</sub> signal was barely monitored in the case of the ionic liquid skinny gels modified Zn (ILG-Zn), alleviating the HER (Figure 10i).<sup>[114]</sup> Apart from the above-mentioned in-situ characterizations, other in-situ techniques (i.e., in-situ XRD, in-situ Raman spectroscopy, in-situ FTIR, in-situ AFM) can also be employed as assisted methods to monitor changes of the Zn anodes.<sup>[115]</sup>

Despite some advanced techniques are applied to explore the interfacial chemistry of Zn anodes, the current understanding of the electrochemical behavior is still limited. Simulations and theoretical calculations are valid tools for simulating electrochemical processes based on corresponding theoretical models, which provide microscopic-level explanations to interpret experimental results. Simulations are powerful tools for modeling various chemical and physical processes by mathematical computations. The finite element method (FEM) is widely used in ZIBs, particularly in simulating the distribution of electric field intensity and ionic concentration on the surface of the Zn anode, which aims to uncover the origins of Zn dendrites during cycling, therefore affording a solid theoretical basis for the development of interfacial engineering.<sup>[116]</sup> For instance, Tian et al explored the favorable conditions for smooth Zn plating in gelatin/sodium alginate-acetate (Gel/SA-acetate) by simulating electric field and Zn<sup>2+</sup> flux distributions.<sup>[117]</sup> The simulation revealed a more uniform electric field distribution and even Zn<sup>2+</sup> concentration gradients in the Gel/SA-acetate hydrogel compared to the liquid electrolyte, indicating that homogeneous electric field and Zn<sup>2+</sup> flux distributions were favorable for achieving stable Zn anodes (Figure 10j-m). Theoretical calculations are primarily based on density functional theory (DFT), which are contributed to the insights into the mechanisms of interfacial engineering from the perspective of charge distribution, migration energy, binding energy, etc., which gain a deeper understanding at the atomic level. Zincophilicity, charge distribution and migration energy acts as crucial parameters in the investigation of diverse strategies to suppress dendrite growth, which can be assessed by the DFT. This approach not only validates experimental observations but also offers theoretical guidance in materials selection, providing robust support for the enhancement of protective strategies. Zhang et al. constructed dense ZnSe nanoparticles on the Zn anodes to eliminate interfacial side reactions and the underlying mechanisms were clarified in detail by DFT.<sup>[118]</sup> The calculated adsorption energy results demonstrated that interactions between Zn atoms and the Zn (001) (-1.136 eV) was stronger than that of ZnSe (111) surface (-0.293 eV), suggesting a lower Zn affinity of ZnSe, which could be attributed to the reduced electron density around the exposed Zn atom of the ZnSe (111) surface bonded with the Se atom. A low Zn affinity of the protective layer ensured that Zn<sup>2+</sup> deposition on the top of coating was unfavorable, thereby invalidating the protection. Moreover, the low migration barriers of the ZnSe (111) (0.76 eV) surface indicated the fast Zn<sup>2+</sup> diffusion kinetics. The origins of improved Zn<sup>2+</sup> migration were uncovered by charge distribution analysis. The Se atoms

interacted with Zn atoms lead to an unbalanced charge distribution, which induced internal driving force to facilitate the fast migration of  $Zn^{2+}$  for achieving even  $Zn^{2+}$  deposition under the protective layer and the suppressing dendrite growth.

## 6. Summary and Perspectives

As a type of energy storage system, ZIBs have been considered as highly promising candidates for application in large-scale energy storage devices. This review briefly summarizes the challenges that plague Zn anodes, including Zn dendrites, HER, corrosion, and passivation. From what has been discussed above, a major emphasis is focused on various interfacial engineering techniques for dendrite-free Zn anodes. In order to get insights into the fundamentals and mechanisms of interfacial engineering, various analytical techniques are introduced. Despite the considerable achievements on Zn anodes by interfacial engineering strategies, there still exist challenges for the further advancement of Zn anodes. Herein, we propose some perspectives for this field:

- (1) The trade-offs of various characteristics: it is important to comprehensively consider the various aspects of the ZIBs. Although some interfacial engineering strategies can effectively inhibit the Zn dendrite and side reactions, the cost of the coating and their effects on electrochemical performances of ZIBs should be considered. For example, a thicker coating will lead to a longer distance and larger resistance, compromising the electrochemical performances. Therefore, it puts forward a higher requirement for interfacial engineering with respect to integrity, thickness, uniformity, and protection effectiveness to obtain a well-balance between the advantages and dendrite growth of ZIBs.
- (2) Formulation of systematic theoretical investigations of Zn anodes: an integrated theoretical system is beneficial to research on the mechanisms of Zn anodes in mild aqueous electrolytes from the molecular or atomic levels. Current reports of the interfacial models are mainly based on alkaline metal anodes, but in fact, the behavior of Zn anode is different from that of alkaline metal anodes. This dilemma has led to confusion in the design of high-performance Zn anodes and has limited the progress of ZIBs. Systematic theoretical investigations will contribute to interpreting construction of stable Zn anodes. It is hence preferable to build appropriate theoretical systems to get in-depth insights into the fundamental principles for the development of this field.
- (3) Establishment of standard test conditions and evaluation criteria of Zn anodes: the absence of uniform testing conditions for Zn anodes makes it hard to establish standard evaluation criteria. Many works have reported that obtained Zn anodes improve their battery performances, but in fact, these results are based on different test conditions, such as current density, electrolyte and DOD, and therefore lack of comparability to some extent.
- (4) Industrialization development: the commercialization of batteries is focused on the cost and energy density. Therefore, the cost of the materials and techniques should be considered to ensure the future industrialization. Despite some coating materials and technologies have made great achievements in the suppression of Zn dendrite and side reactions, they cannot meet practical requirements. For example, Nafion-zeolite coatings demonstrate their excellent performance, but they are expensive for large-scale. They will increase the manufacturing cost of ZIBs that are uneconomical for industrial production. Meanwhile, attention should be paid to the mass loading of the electrodes. The electrodes typically contain the low mass loading of active material (about 1 mg/cm<sup>2</sup>) for lab-scale measurements, which can yield favorable electrochemical performances. However, a realistic evaluation of ZIBs needs active mass loading of electrodes at least 7–10 mg/cm<sup>2</sup>. It is imperative to assess the holistic performance under these working conditions.
- (5) Development of novel coating materials and methods: advanced coating materials, particularly those based on polymers, must be innovatively designed to address the challenges associated with poor conductivity, uniform active sites, and favorable hydrophilicity. Considering the intricate interactions of various coatings and chemical bonds, it is essential to explore the realm of multi-component coating materials. For instance, the exploration of double-layer coatings, incorporating both an electronic conductor layer and an ionic conductor, shows great potential for enhancing the stability of Zn anodes, which capitalizes on the synergistic effects by the interaction of two essential components. The electronic conductor layer applied to the Zn anode surface establishes a more uniform electric field, while the ionic conductor contributes to the confinement of Zn ions.
- (6) Integration of different strategies: many approaches aimed at preventing dendrite formation on Zn anodes often focus on individual strategy such as surface modification or electrolyte design. However, the effect of each strategy has its inherent limitations and most of reports are only focused on one method. Optimizations need to address multiple challenges through the integration of combined strategies simultaneously. These strategies should be integrated to ensure mass production feasibility without compromising cost-effectiveness. For instance, incorporating economical electrolyte additives for ion flux, coupled with a surface coating for physical shielding and corrosion prevention, endows the Zn anodes with long-term stability.

Furthermore, the lifespan of symmetric cells may not be reliable owing to the existence of soft short-circuits. And it should be noted that the real working conditions of the ZIBs should be chosen for testing, such as appropriate current rates. On the other hand, the reproducibility of the experimental data should be ensured. Hence, it is a key to formulating some specific test protocol standards to obtain meaningful data of actual ZIBs.

## Acknowledgements

This work is financially supported by the National Natural Science Foundation of China (22272150), the Major Program of Zhejiang Provincial Natural Science Foundation of China (LD22B030002 and LZ23B030002), and Zhejiang Provincial Ten Thousand Talent Program (2021R51009). W. Lu acknowledges the Key Science and Technology Project of Jinhua City (KYZ04Y22378).

## Conflict of Interests

The authors declare no conflict of interest.

**Keywords:** interfacial engineering · Zn anodes · Zn dendrites · side reactions · aqueous Zn-ion batteries

- [1] a) L. Kang, J. Zheng, K. Yue, H. Yuan, J. Luo, Y. Wang, Y. Liu, J. Nai, X. Tao, *Small* **2023**, *19*, 202304094; b) P. H. Chen, W. Y. Zhou, Z. J. Xiao, S. Q. Li, Z. B. Wang, Y. C. Wang, S. S. Xie, *Nano Energy* **2020**, *74*, 104905; c) X. Zhou, P. Cao, A. Wei, A. Zou, H. Ye, W. Liu, J. Tang, J. Yang, *ACS Appl. Mater. Inter.* **2021**, *13*, 8181.
- [2] a) Y. Liu, C. Wang, S. G. Yoon, S. Y. Han, J. A. Lewis, D. Prakash, E. J. Klein, T. Chen, D. H. Kang, D. Majumdar, R. Gopalaswamy, M. T. McDowell, *Nat. Commun.* **2023**, *14*, 3975; b) S. Zhang, H. Yu, Y. Gao, K. Zhu, H. Wu, D. Cao, *Composites Part B* **2023**, *264*, 110932; c) Z. Li, M. Du, X. Guo, D. Zhang, Q. Wang, H. Sun, B. Wang, Y. A. Wu, *Chem. Eng. J.* **2023**, *473*, 145294.
- [3] Y. Lai, T. Yang, Y. Wang, W. Li, Y. Xie, S. Cheng, L. Qiao, X. Wang, *Chem. Eng. J.* **2023**, *462*, 142223.
- [4] a) X. Luan, L. Qi, Z. Zheng, Y. Gao, Y. Xue, Y. Li, *Angew. Chem. Int. Ed.* **2023**, *62*, e202215968; b) J. D. Guan, Q. F. Huang, L. Y. Shao, X. Y. Shi, D. D. Zhao, L. B. Wang, Z. P. Sun, *Small* **2023**, *19*, 2207148; c) Q. Wen, H. Fu, R. d. Cui, H. Z. Chen, R. H. Ji, L. B. Tang, C. Yan, J. Mao, K. H. Dai, X. H. Zhang, J. C. Zheng, *J. Energy Chem.* **2023**, *83*, 287; d) R. Zhao, J. Yang, X. Han, Y. Wang, Q. Ni, Z. Hu, C. Wu, Y. Bai, *Adv. Energy Mater.* **2023**, *13*, 2203542; e) Y. Liu, Y. Liu, X. Wu, Y. R. Cho, *J. Colloid Interf. Sci.* **2022**, *628*, 33.
- [5] a) Y. Zong, H. He, Y. Wang, M. Wu, X. Ren, Z. Bai, N. Wang, X. Ning, S. X. Dou, *Adv. Energy Mater.* **2023**, *13*, 2300403; b) W. Ye, P. Ye, H. Wang, F. Chen, Y. Zhong, Y. Hu, *J. Colloid Interf. Sci.* **2022**, *612*, 298.
- [6] a) N. Zhang, J. C. Wang, Y. F. Guo, P. F. Wang, Y. R. Zhu, T. F. Yi, *Coord. Chem. Rev.* **2023**, *479*, 215009; b) X. Wu, C. Yin, M. Zhang, Y. Xie, J. Hu, R. Long, X. Wu, X. Wu, *Chem. Eng. J.* **2023**, *452*, 139573; c) Q. Zong, Y. Zhuang, C. Liu, Q. Kang, Y. Wu, J. Zhang, J. Wang, D. Tao, Q. Zhang, G. Cao, *Adv. Energy Mater.* **2023**, *13*, 2301480; d) J. Gu, H. Wang, S. Li, M. Sohail Riaz, J. Ning, X. Pu, Y. Hu, *J. Colloid Interf. Sci.* **2023**, *635*, 254; e) Z. Xu, L. Yan, J. Shen, X. Yang, J. Ning, Y. Zhong, Y. Hu, *Sci. China Technol. Sc.* **2022**, *65*, 693.
- [7] a) H. Qin, W. Chen, W. Kuang, N. Hu, X. Zhang, H. Weng, H. Tang, D. Huang, J. Xu, H. He, *Small* **2023**, *19*, 2300130; b) L. Yan, B. Xie, C. Yang, Y. Wang, J. Ning, Y. Zhong, Y. Hu, *Adv. Energy Mater.* **2023**, *13*, 2204245; c) W. Lu, B. B. Xie, C. Yang, C. Tian, L. Yan, J. Ning, S. Li, Y. Zhong, Y. Hu, *Small* **2023**, *19*, 2302629; d) W. Lu, Y. Yang, T. Zhang, L. Ma, X. Luo, C. Huang, J. Ning, Y. Zhong, Y. Hu, *J. Colloid Interf. Sci.* **2021**, *590*, 226; e) Q. Li, W. Lu, Z. Li, J. Ning, Y. Zhong, Y. Hu, *Chem. Eng. J.* **2020**, *380*, 122544.
- [8] a) L. Wu, Y. Dong, *Energy Storage Mater.* **2021**, *41*, 715; b) Y. Ren, P. Ye, J. Chen, H. Wang, J. Ning, J. Shen, Y. Zhong, Y. Hu, *J. Power Sources* **2022**, *545*, 231908; c) K. Wang, J. Hu, T. Chen, K. Wang, J. Wu, Q. Chen, Z. Deng, W. Zhang, *ACS Sustainable Chem. Eng.* **2023**, *11*, 9111; d) A. Konarov, N. Voronina, J. H. Jo, Z. Bakenov, Y. K. Sun, S. T. Myung, *ACS Energy Lett.* **2018**, *3*, 2620.
- [9] a) A. Zhang, R. Zhao, Y. Wang, J. Yang, C. Wu, Y. Bai, *Energy Environ. Sci.* **2023**, *16*, 3240; b) Y. Liu, X. Wu, *J. EnergyChem* **2023**, *87*, 334.
- [10] a) Y. Liu, Y. Liu, X. Wu, Y. R. Cho, *ACS Sustainable Chem. Eng.* **2023**, *11*, 13298; b) Y. Liu, Y. Liu, X. Wu, *Chin. Chem. Lett.* **2023**, *34*, 107839.
- [11] M. Li, M. Maisuradze, R. Sciacca, I. Hasa, M. Giorgetti, *Batteries Supercaps* **2023**, *6*, e202300340.
- [12] E. Grignon, A. M. Battaglia, T. B. Schon, D. S. Seferos, *iScience* **2022**, *25*, 104204.
- [13] a) P. Cai, K. L. Wang, J. Ning, X. He, M. L. Chen, Q. X. Li, H. M. Li, M. Zhou, W. Wang, K. Jiang, *Adv. Energy Mater.* **2022**, *12*, 2202182; b) L. Li, S. Jia, M. Cao, Y. Ji, H. Qiu, D. Zhang, *Chin. Chem. Lett.* **2023**, *34*, 108307; c) W. Shi, Z. Song, J. Wang, Q. Li, Q. An, *Chem. Eng. J.* **2022**, *446*, 137295; d) Q. Wen, H. Fu, Z. Wang, Y. Huang, Z. He, C. Yan, J. Mao, K. Dai, X. Zhang, J. Zheng, *J. Mater. Chem. A* **2022**, *10*, 17501; e) L. Yan, H. Wang, J. Shen, J. Ning, Y. Zhong, Y. Hu, *Chem. Eng. J.* **2021**, *403*, 126385.
- [14] a) H. Li, B. Chen, R. Gao, F. Xu, X. Wen, X. Zhong, C. Li, Z. Piao, N. Hu, X. Xiao, F. Shao, G. Zhou, J. Yang, *Nano Res.* **2023**, *16*, 4933; b) H. Wang, M. S. Riaz, T. Ali, J. Gu, Y. Zhong, Y. Hu, *Small Sci.* **2023**, *3*, 2200104; c) W. Lu, L. Yan, W. Ye, J. Ning, Y. Zhong, Y. Hu, *J. Mater. Chem. A* **2022**, *10*, 15267; d) H. Wang, Y. Zhong, J. Ning, Y. Hu, *Chin. Chem. Lett.* **2021**, *32*, 3733.
- [15] a) H. Wang, W. Ye, B. Yin, K. Wang, M. S. Riaz, B. B. Xie, Y. Zhong, Y. Hu, *Angew. Chem. Int. Ed.* **2023**, *62*, e202218872; b) J. W. Gu, Z. Yuan, H. Y. Wang, J. L. Shen, J. Q. Ning, Y. J. Zhong, Y. Hu, *Chem. Eng. J.* **2022**, *448*, 137711; c) L. Yan, Z. Xu, X. Liu, S. Mahmood, J. Shen, J. Ning, S. Li, Y. Zhong, Y. Hu, *Chem. Eng. J.* **2022**, *446*, 137049; d) F. Li, D. Ma, K. Ouyang, M. Yang, J. Qiu, J. Feng, Y. Wang, H. Mi, S. Sun, L. Sun, C. He, P. Zhang, *Adv. Energy Mater.* **2023**, *13*, 2204365; e) T. Li, S. Yan, H. Dong, Y. Zheng, K. Ming, Z. Tong, G. Li, H. Li, W. Li, Q. Wang, J. Liu, Y. Wang, *J. Colloid Interf. Sci.* **2023**, *651*, 959.
- [16] a) R. Wang, S. Xin, D. Chao, Z. Liu, J. Wan, P. Xiong, Q. Luo, K. Hua, J. Hao, C. Zhang, *Adv. Funct. Mater.* **2022**, *32*, 2207751; b) B. Li, S. Liu, Y. Geng, C. Mao, L. Dai, L. Wang, S. C. Jun, B. Lu, Z. He, J. Zhou, *Adv. Funct. Mater.* **2023**, <https://doi.org/10.1002/adfm.202214033>; c) W. Ye, H. Wang, J. Shen, S. Khan, Y. Zhong, J. Ning, Y. Hu, *Chin. Chem. Lett.* **2023**, *34*, 107198; d) Y. Yang, D. Chen, H. Wang, P. Ye, Z. Ping, J. Ning, Y. Zhong, Y. Hu, *Chem. Eng. J.* **2022**, *431*, 133250; e) L. Zhou, Y. Yang, J. Yang, P. Ye, T. Ali, H. Wang, J. Ning, Y. Zhong, Y. Hu, *Appl. Surf. Sci.* **2022**, *604*, 154526.
- [17] X. Zhang, J. P. Hu, N. Fu, W. B. Zhou, B. Liu, Q. Deng, X. W. Wu, *InfoMat.* **2022**, *4*, e12306.
- [18] a) B. Li, X. Zhang, T. Wang, Z. He, B. Lu, S. Liang, J. Zhou, *Nano-Micro Lett.* **2021**, *14*, 6; b) Q. Zhang, Y. Su, Z. Shi, X. Yang, J. Sun, *Small* **2022**, *18*, 2203583; c) H. Wang, C. Wang, Y. Tang, *EcoMat* **2021**, *3*, e12172.
- [19] a) J. Zheng, Z. Huang, F. Ming, Y. Zeng, B. Wei, Q. Jiang, Z. Qi, Z. Wang, H. Liang, *Small* **2022**, *18*, 2200006; b) M. Liu, W. Yuan, G. Ma, K. Qiu, X. Nie, Y. Liu, S. Shen, N. Zhang, *Angew. Chem. Int. Ed.* **2023**, *62*, e202304444; c) J. Zhu, Z. Bie, X. Cai, Z. Jiao, Z. Wang, J. Tao, W. Song, H. J. Fan, *Adv. Mater.* **2022**, *34*, 2207209; d) Z. Wang, X. Zhu, K. Wang, Z. Huang, J. Chen, *ACS Appl. Mater. Inter.* **2023**, *15*, 31449; e) H. Wang, X. Chen, J. Zhang, Z. Yuan, P. Ye, J. Shen, Y. Zhong, Y. Hu, *Appl. Surf. Sci.* **2022**, *598*, 153819; f) D. Yao, D. Yu, S. Yao, Z. Lu, G. Li, H. Xu, F. Du, *ACS Appl. Mater. Inter.* **2023**, *15*, 16584.
- [20] X. Zhang, H. Luo, Y. Guo, C. Xu, Y. Deng, Z. Deng, Y. Zhang, H. Wu, W. Cai, Y. Zhang, *Chem. Eng. J.* **2023**, *457*, 141305.
- [21] a) W. Nie, H. Cheng, Q. Sun, S. Liang, X. Lu, B. Lu, J. Zhou, *Small Methods* **2023**, <https://doi.org/10.1002/smtd.202201572>; b) C. Nie, G. Wang, D. Wang, M. Wang, X. Gao, Z. Bai, N. Wang, J. Yang, Z. Xing, S. Dou, *Adv. Energy Mater.* **2023**, *13*, 2300606.
- [22] a) J. Z. Fu, Y. P. Guo, H. W. Wang, P. Xiao, J. N. Liang, Q. F. Sun, H. Q. Li, *Energy Storage Mater.* **2023**, *61*, 102856; b) X. Fu, G. Li, X. Wang, J. Wang, W. Yu, X. Dong, D. Liu, *J. Energy Chem.* **2024**, *88*, 125; c) X. Liu, H. Wang, X. Fan, Q. Wang, J. Liu, W. Xu, Z. Wu, J. Wan, C. Zhong, W. Hu, *Energy Storage Mater.* **2023**, *58*, 311; d) X. Xie, S. Liang, J. Gao, S. Guo, J. Guo, C. Wang, G. Xu, X. Wu, G. Chen, J. Zhou, *Energy Environ. Sci.* **2020**, *13*, 503.
- [23] a) T. B. Song, Q. L. Ma, X. R. Zhang, J. W. Ni, T. L. He, H. M. Xiong, *Chem. Eng. J.* **2023**, *471*, 144735; b) Z. Meng, Y. Jiao, P. Wu, *Angew. Chem. Int. Ed.* **2023**, *62*, e202307271; c) Y. Zeng, Z. Pei, D. Luan, X. W. D. Lou, J. Am. Chem. Soc. **2023**, *145*, 12333; d) Y. Chen, W. L. Wang, W. B. Zhao, J. T. Xu, P. H. Shi, Y. L. Min, *J. Colloid Interf. Sci.* **2023**, *650*, 593.
- [24] a) M. Liu, L. Yao, Y. Ji, M. Zhang, Y. Gan, Y. Cai, H. Li, W. Zhao, Y. Zhao, Z. Zou, R. Qin, Y. Wang, L. Liu, H. Liu, K. Yang, T. S. Miller, F. Pan, J. Yang, *Nano Lett.* **2023**, *23*, 541; b) Q. Zhang, J. Luan, Y. Tang, X. Ji, H. Wang, *Angew. Chem. Int. Ed.* **2020**, *59*, 13180; c) P. H. Cao, J. J. Tang, A. R. Wei, Q. X. Bai, Q. Meng, S. C. Fan, H. Ye, Y. L. Zhou, X. Y. Zhou, J. Yang, *ACS Appl. Mater. Inter.* **2021**, *13*, 48855; d) W. Ye, H. Wang, J. Ning, Y. Zhong, Y. Hu, *J. Energy Chem.* **2021**, *57*, 219; e) H. Wang, Y.

- Yang, Q. Li, W. Lu, J. Ning, Y. Zhong, Z. Zhang, Y. Hu, *Sci. China Mater.* **2021**, *64*, 840.
- [25] V. Yufit, F. Tariq, D. S. Eastwood, M. Biton, B. Wu, P. D. Lee, N. P. Brandon, *Joule* **2019**, *3*, 485.
- [26] a) M. Kim, S. J. Shin, J. Lee, Y. Park, Y. Kim, H. Kim, J. W. Choi, *Angew. Chem. Int. Ed.* **2022**, *61*, e202211589; b) D. Li, Y. Tang, S. Liang, B. Lu, G. Chen, J. Zhou, *Energy Environ. Sci.* **2023**, *16*, 3381.
- [27] a) S. Xie, Y. Li, L. Dong, *J. Energy Chem.* **2023**, *76*, 32; b) N. Wang, Y. Zhang, J. Yuan, L. Hu, M. Sun, Z. Li, X. Yao, X. Weng, C. Jia, *ACS Appl. Mater. Inter.* **2022**, *14*, 48081; c) C. Huang, W. Deng, X. Yuan, Y. Zhou, C. Li, J. Hu, M. Zhang, J. Zhu, R. Li, *ACS Appl. Mater. Inter.* **2023**, *15*, 2341.
- [28] a) T. Chen, F. Huang, Y. N. Wang, Y. Yang, H. Tian, J. M. Xue, *Adv. Sci.* **2022**, *9*, 2105980; b) S. Jin, J. Yin, X. Gao, A. Sharma, P. Chen, S. Hong, Q. Zhao, J. Zheng, Y. Deng, Y. L. Joo, L. A. Archer, *Nat. Commun.* **2022**, *13*, 2283; c) Y. Xu, X. Zheng, J. Sun, W. Wang, M. Wang, Y. Yuan, M. Chuai, N. Chen, H. Hu, W. Chen, *Nano Lett.* **2022**, *22*, 3298.
- [29] a) S. So, Y. N. Ahn, J. Ko, I. T. Kim, J. Hur, *Energy Storage Mater.* **2022**, *52*, 40; b) Y. Sun, Q. Jian, T. Wang, B. Liu, Y. Wan, J. Sun, T. Zhao, *J. Energy Chem.* **2023**, *81*, 583; c) S. Tao, C. Zhang, J. Zhang, Y. Jiao, M. Li, W. Lin, L. Ran, B. Clement, M. Lyu, I. Gentle, L. Wang, R. Knibbe, *Chem. Eng. J.* **2022**, *446*, 136607; d) H. Ying, P. Huang, Z. Zhang, S. Zhang, Q. Han, Z. Zhang, J. Wang, W. Q. Han, *Nano-Micro Lett.* **2022**, *14*, 180.
- [30] a) A. Bayaguud, Y. Fu, C. Zhu, *J. Energy Chem.* **2022**, *64*, 246; b) D. L. Han, Z. X. Wang, H. T. Lu, H. Li, C. J. Cui, Z. C. Zhang, R. Sun, C. N. Geng, Q. H. Liang, X. X. Guo, Y. B. Mo, X. Zhi, F. Y. Kang, Z. Weng, Q. H. Yang, *Adv. Energy Mater.* **2022**, *12*, 2102982; c) J. B. Park, C. Choi, J. H. Park, S. Yu, D. W. Kim, *Adv. Energy Mater.* **2022**, *12*, 2202937; d) X. Zheng, Z. Liu, J. Sun, R. Luo, K. Xu, M. Si, J. Kang, Y. Yuan, S. Liu, T. Ahmad, T. Jiang, N. Chen, M. Wang, Y. Xu, M. Chuai, Z. Zhu, Q. Peng, Y. Meng, K. Zhang, W. Wang, W. Chen, *Nat. Commun.* **2023**, *14*, 76.
- [31] a) A. Krężel, W. Maret, *Arch. Biochem. Biophys.* **2016**, *611*, 3.
- [32] Q. Zhang, X. Liu, X. Zhu, Y. Wan, C. Zhong, *Small Methods* **2023**, *7*, 2201277.
- [33] Z. Yi, G. Chen, F. Hou, L. Wang, J. Liang, *Adv. Energy Mater.* **2021**, *11*, 2003065.
- [34] X. Wang, C. Sun, Z.-S. Wu, *SusMat* **2023**, *3*, 180.
- [35] H. Li, S. Guo, H. Zhou, *Energy Storage Mater.* **2023**, *56*, 227.
- [36] J. Zhao, J. Zhang, W. Yang, B. Chen, Z. Zhao, H. Qiu, S. Dong, X. Zhou, G. Cui, L. Chen, *Nano Energy* **2019**, *57*, 625.
- [37] a) X. Bai, Y. Nan, K. Yang, B. J. Deng, J. J. Shao, W. G. Hu, X. Pu, *Adv. Funct. Mater.* **2023**, *33*, 202307595; b) P. Kulkarni, S. S. Kim, H. Y. Jung, *J. Energy Chem.* **2023**, *86*, 1; c) Z. Wang, L. Li, F. Zhao, S. Gong, H. Xu, M. Li, B. Yekeping, R. Li, J. Qi, H. Wang, C. Li, W. Peng, J. Liu, *J. Colloid Interf. Sci.* **2023**, *645*, 542.
- [38] H. F. Fan, M. Li, E. D. Wang, *Nano Energy* **2022**, *103*, 107751.
- [39] a) C. Li, X. Xie, S. Liang, J. Zhou, *Energy Environ. Mater.* **2020**, *3*, 146.
- [40] a) Y. Liang, Y. Wang, H. Mi, L. Sun, D. Ma, H. Li, C. He, P. Zhang, *Chem. Eng. J.* **2021**, *425*, 131862; b) H. Jia, Z. Wang, M. Dirican, S. Qiu, C. Y. Chan, S. Fu, B. Fei, X. Zhang, J. Mater. Chem. A **2021**, *9*, 5597; c) S. Tian, L. Zhou, W. He, Y. Tian, Y. Zhou, S. Wu, R. Jian, K. J. Balkus, T. Luo, G. Xiong, *Chem. Eng. J.* **2023**, *462*, 142276; d) B. Zhou, B. Miao, Y. Gao, A. Yu, Z. Shao, *Small* **2023**, *19*, 2300895; e) L. Pan, H. He, Q. Yan, P. Hu, *Power Sources* **2023**, *571*, 233090.
- [41] a) Q. Ren, X. Tang, X. Zhao, Y. Wang, C. Li, S. Wang, Y. Yuan, *Nano Energy* **2023**, *109*, 108306; b) Z. Hu, L. Zhou, D. Meng, L. Zhao, W. Wang, Y. Li, Y. Huang, Y. Wu, S. Yang, L. Li, Z. Hong, *ACS Appl. Mater. Inter.* **2023**, *15*, 5161; c) M. Li, X. Zhou, X. He, C. Lai, B. Shan, K. Wang, K. Jiang, *ACS Appl. Mater. Inter.* **2023**, *15*, 3017.
- [42] a) L. Hong, X. Wu, C. Ma, W. Huang, Y. Zhou, K. X. Wang, J. S. Chen, *J. Mater. Chem. A* **2021**, *9*, 16814; b) Y. Zhou, W. Li, Y. Xie, L. Deng, B. Ke, Y. Jian, S. Cheng, B. Qu, X. Wang, *ACS Appl. Mater. Inter.* **2023**, *15*, 9486.
- [43] a) W. Hu, J. Ju, N. Deng, M. Liu, W. Liu, Y. Zhang, L. Fan, W. Kang, B. Cheng, *J. Mater. Chem. A* **2021**, *9*, 25750; b) L. Liu, J. Cheng, X. Wang, J. Zhang, B. Wang, *ACS Appl. Mater. Inter.* **2023**, *15*, 31867.
- [44] a) Q. Hu, J. Hou, Y. Liu, L. Li, Q. Ran, J. Mao, X. Liu, J. Zhao, H. Pang, *Adv. Mater.* **2023**, *35*, 2303336; b) Y. G. Feng, Y. D. Wang, L. Sun, K. Q. Zhang, J. C. Liang, M. F. Zhu, Z. X. Tie, Z. Jin, *Small* **2023**, *19*, 2302650; c) G. Jiang, R. Xue, L. He, J. Zhu, N. Qiu, Y. Wang, *Chem. Eng. J.* **2023**, *472*, 145016; d) J. Zhou, Q. Li, X. Hu, W. Wei, X. Ji, G. Kuang, L. Zhou, L. Chen, Y. Chen, *Chin. Chem. Lett.* **2023**, <https://doi.org/10.1016/j.ccl.2023.109143>; e) J. P. Chen, W. Y. Zhao, J. M. Jiang, X. L. Zhao, S. H. Zheng, Z. H. Pan, X. W. Yang, *Energy Storage Mater.* **2023**, *59*, 102767.
- [45] Y. Song, L. Wang, L. Sheng, D. Ren, H. Liang, Y. Li, A. Wang, H. Zhang, H. Xu, X. He, *Energy Environ. Sci.* **2023**, *16*, 1943.
- [46] H. Chen, X. Li, K. Fang, H. Wang, J. Ning, Y. Hu, *Adv. Energy Mater.* **2023**, *13*, 2302187.
- [47] B. Sun, P. Xiong, U. Maitra, D. Langsdorf, K. Yan, C. Wang, J. Janek, D. Schröder, G. Wang, *Adv. Mater.* **2020**, *32*, 1903891.
- [48] H. Yu, Z. Wang, R. Zheng, L. Yan, L. Zhang, J. J. A. C. Shu, *Angew. Chem. Int. Ed.* **2023**, *135*, e202308397.
- [49] L. Yao, C. Hou, M. Liu, H. Chen, Q. Zhao, Y. Zhao, Y. Wang, L. Liu, Z. W. Yin, J. Qiu, S. Li, R. Qin, F. Pan, *Adv. Funct. Mater.* **2023**, *33*, 2209301.
- [50] a) B. He, H. Y. Qin, J. Wu, X. F. Chen, R. S. Huang, F. Shen, Z. R. Wu, G. N. Chen, S. B. Yin, J. Liu, *Energy Storage Mater.* **2021**, *43*, 317; b) Z. Zhou, Z. Chen, X. Luo, L. Wang, J. Liang, W. Peng, Y. Li, F. Zhang, X. Fan, *ACS Appl. Mater. Inter.* **2022**, *14*, 24386.
- [51] F. Tao, Y. Liu, X. Ren, J. Wang, Y. Zhou, Y. Miao, F. Ren, S. Wei, J. Ma, *J. Energy Chem.* **2022**, *66*, 397.
- [52] R. Qin, Y. Wang, L. Yao, L. Yang, Q. Zhao, S. Ding, L. Liu, F. Pan, *Nano Energy* **2022**, *98*, 107333.
- [53] W. Wu, Y. Deng, G. Chen, *Chin. Chem. Lett.* **2023**, *34*, 108424.
- [54] Y. Mao, Z. Li, Y. Li, D. Cao, G. Wang, K. Zhu, G. Chen, *Chem. Eng. J.* **2023**, *461*, 141707.
- [55] J. Yang, R. Zhao, Y. Wang, Z. Hu, Y. Wang, A. Zhang, C. Wu, Y. Bai, *Adv. Funct. Mater.* **2023**, *33*, 2213510.
- [56] B. Li, X. Zhang, T. Wang, Z. He, B. Lu, S. Liang, J. Zhou, *Nano-Micro Lett.* **2021**, *14*, 6.
- [57] L. T. Hieu, S. So, I. T. Kim, J. Hur, *Chem. Eng. J.* **2021**, *411*, 128584.
- [58] S. Zheng, L. Wei, Z. Zhang, J. Pan, J. He, L. Gao, C. C. Li, *Nano Lett.* **2022**, *22*, 9062.
- [59] A. Naveed, T. Rasheed, B. Raza, J. Chen, J. Yang, N. Yanna, J. Wang, *Energy Storage Mater.* **2022**, *44*, 206.
- [60] Z. Xing, Y. Sun, X. Xie, Y. Tang, G. Xu, J. Han, B. Lu, S. Liang, G. Chen, J. Zhou, *Angew. Chem. Int. Ed.* **2023**, *62*, e202215324.
- [61] Y. Z. Chu, L. X. Ren, Z. L. Hu, C. D. Huang, J. Y. Luo, *Green Energy Environ.* **2023**, *8*, 1006.
- [62] Y. Yang, C. Liu, Z. Lv, H. Yang, Y. Zhang, M. Ye, L. Chen, J. Zhao, C. C. Li, *Adv. Mater.* **2021**, *33*, 2007388.
- [63] P. H. Cao, X. Y. Zhou, A. R. Wei, Q. Meng, H. Ye, W. P. Liu, J. J. Tang, J. Yang, *Adv. Funct. Mater.* **2021**, *31*, 2100398.
- [64] P. Xiong, Y. Zhang, J. Zhang, S. H. Baek, L. Zeng, Y. Yao, H. S. Park, *EnergyChem* **2022**, *4*, 100076.
- [65] J. Zheng, Z. Huang, Y. Zeng, W. Liu, B. Wei, Z. Qi, Z. Wang, C. Xia, H. Liang, *Nano Lett.* **2022**, *22*, 1017.
- [66] M. W. Cui, Y. Xiao, L. T. Kang, W. Du, Y. F. Gao, X. Q. Sun, Y. L. Zhou, X. M. Li, H. F. Li, F. Y. Jiang, C. Y. Zhi, *ACS Appl. Energ. Mater.* **2019**, *2*, 6490.
- [67] J. L. Yang, L. Liu, Z. Yu, P. Chen, J. Li, P. A. Dananjaya, E. K. Koh, W. S. Lev, K. Liu, P. Yang, H. J. Fan, *ACS Energy Lett.* **2023**, *8*, 2042.
- [68] X. Y. Guo, G. J. He, *J. Mater. Chem. A* **2023**, *11*, 11987.
- [69] X. Yang, C. Li, Z. Sun, S. Yang, Z. Shi, R. Huang, B. Liu, S. Li, Y. Wu, M. Wang, Y. Su, S. Dou, J. Sun, *Adv. Mater.* **2021**, *33*, 2105951.
- [70] X. Song, L. Bai, C. Wang, D. Wang, K. Xu, J. Dong, Y. Li, Q. Shen, J. Yang, *ACS Nano* **2023**, *17*, 15113.
- [71] Y. Liu, T. Guo, Q. Liu, F. Xiong, M. Huang, Y. An, J. Wang, Q. An, C. Liu, L. Mai, *Mater. Today Energy* **2022**, *28*, 101056.
- [72] T. Wang, C. Li, X. Xie, B. Lu, Z. He, S. Liang, J. Zhou, *ACS Nano* **2020**, *14*, 16321.
- [73] S. H. Lee, J. Han, T. W. Cho, G. H. Kim, Y. J. Yoo, J. Park, Y. J. Kim, E. J. Lee, S. Lee, S. M. Mhin, S. Y. Park, J. Yoo, S. H. Lee, *Nanoscale* **2023**, *15*, 3737.
- [74] H. B. He, J. Liu, *J. Mater. Chem. A* **2020**, *8*, 22100.
- [75] P. Liu, Z. Zhang, R. Hao, Y. Huang, W. Liu, Y. Tan, P. Li, J. Yan, K. Liu, *Chem. Eng. J.* **2021**, *403*, 126425.
- [76] M. Idrees, S. Batool, J. Cao, M. S. Javed, S. Xiong, C. Liu, Z. Chen, *Nano Energy* **2022**, *100*, 107505.
- [77] A. Chen, C. Zhao, J. Gao, Z. Guo, X. Lu, J. Zhang, Z. Liu, M. Wang, N. Liu, L. Fan, Y. Zhang, N. Zhang, *Energy Environ. Sci.* **2023**, *16*, 275.
- [78] T. Huang, K. Xu, N. Jia, L. Yang, H. Liu, J. Zhu, Q. Yan, *Adv. Mater.* **2023**, *35*, 2205206.
- [79] Z. Li, L. Wu, S. Dong, T. Xu, S. Li, Y. An, J. Jiang, X. Zhang, *Adv. Funct. Mater.* **2021**, *31*, 2006495.
- [80] C. Guo, J. Zhou, Y. T. Chen, H. F. Zhuang, J. Li, J. L. Huang, Y. L. Zhang, Y. F. Chen, S. L. Li, Y. Q. Lan, *Angew. Chem. Int. Ed.* **2023**, *62*, e202300125.
- [81] J. Li, K. Le, W. Wei, *J. Mater. Sci. Technol.* **2022**, *102*, 272.
- [82] Q. Gou, Z. Chen, H. Luo, J. Deng, B. Zhang, N. Xu, J. Cui, Y. Zheng, M. Li, J. Li, *Small* **2023**, <https://doi.org/10.1002/smll.202305902>.

- [83] Z. F. Ge, H. Zhang, J. Z. Tian, J. E. Wu, Y. L. Xu, W. T. Deng, G. Q. Zou, D. He, H. S. Hou, C. R. Wang, X. B. Ji, *Chem. Eng. J.* **2023**, *466*, 143054.
- [84] X. Zhou, R. Chen, E. Cui, Q. Liu, H. Zhang, J. Deng, N. Zhang, C. Xie, L. Xu, L. Mai, *Energy Storage Mater.* **2023**, *55*, 538.
- [85] J. Ko, S. So, M. Kim, I. Tae Kim, Y. Nam Ahn, J. Hur, *Chem. Eng. J.* **2023**, *462*, 142308.
- [86] P. Li, J. Ren, C. Li, J. Li, K. Zhang, T. Wu, B. Li, L. Wang, *Chem. Eng. J.* **2023**, *451*, 138769.
- [87] X. Yang, J. Lv, C. Cheng, Z. Shi, J. Peng, Z. Chen, X. Lian, W. Li, Y. Zou, Y. Zhao, M. H. Rümmeli, S. Dou, J. Sun, *Adv. Sci.* **2023**, *10*, 2206077.
- [88] H. Jia, M. Qiu, C. Tang, H. Liu, S. Fu, X. Zhang, *EcoMat* **2022**, *4*, e12190.
- [89] L. Sun, Y. Wang, G. Duan, B. Luo, S. Zheng, J. Huang, Z. Ye, *J. Mater. Chem. A* **2023**, *11*, 17188.
- [90] S. H. Gong, H. J. Lim, J. H. Lee, Y. Yoo, S. Yu, H. D. Lim, H. W. Jung, J. S. Ko, I. S. Kim, H. S. Kim, *Appl. Surf. Sci.* **2023**, *611*, 155633.
- [91] G. Zhu, H. Zhang, J. Lu, Y. Hou, P. Liu, S. Dong, H. Pang, Y. Zhang, *Adv. Funct. Mater.* **2023**, <https://doi.org/10.1002/adfm.20230>.
- [92] a) Z. Shi, M. Yang, Y. Ren, Y. Wang, J. Guo, J. Yin, F. Lai, W. Zhang, S. Chen, H. N. Alshareef, T. Liu, *ACS Nano* **2023**, *17*, 21893; b) Y. Li, Q. Zhu, M. Xu, B. Zang, Y. Wang, B. Xu, *Adv. Funct. Mater.* **2023**, *33*, 2213416.
- [93] a) Q. Zong, B. Lv, C. Liu, Y. Yu, Q. Kang, D. Li, Z. Zhu, D. Tao, J. Zhang, J. Wang, Q. Zhang, G. Cao, *ACS Energy Lett.* **2023**, *8*, 2886; b) Y. Zhu, Z. Huang, M. Zheng, H. Chen, S. Qian, C. Sun, Y. Tian, Z. Wu, C. Lai, S. Zhang, Y. L. Zhong, *Adv. Funct. Mater.* **2023**, <https://doi.org/10.1002/adfm.202306085>.
- [94] Z. Jiang, K. Yin, R. Pan, G. Zhang, F. Cui, K. Luo, Y. Xiong, L. Sun, *Small* **2023**, *19*, 2302995.
- [95] a) Y. Tang, J. H. Li, C.-L. Xu, M. Liu, B. Xiao, P. F. Wang, *Carbon Neutralization* **2023**, *2*, 186; b) J. Yin, X. Feng, Z. Gan, Y. Gao, Y. Cheng, X. Xu, *Energy Storage Mater.* **2023**, *54*, 623.
- [96] X. Yang, J. Lv, C. Cheng, Z. Shi, J. Peng, Z. Chen, X. Lian, W. Li, Y. Zou, Y. Zhao, M. H. Rümmeli, S. Dou, J. Sun, *Adv. Sci.* **2023**, *10*, 2206077.
- [97] J. C. Bürger, S. Lee, J. Büttner, S. Gutsch, M. Kolhep, A. Fischer, F. M. Ross, M. Zacharias, *ACS Appl. Mater. Inter.* **2023**, *15*, 28387.
- [98] A. Chen, C. Zhao, J. Gao, Z. Guo, X. Lu, J. Zhang, Z. Liu, M. Wang, N. Liu, L. Fan, Y. Zhang, N. Zhang, *Energy Environ. Sci.* **2023**, *16*, 275.
- [99] Y. Lyu, J. A. Yuwono, P. Wang, Y. Wang, F. Yang, S. Liu, S. Zhang, B. Wang, K. Davey, J. Mao, Z. Guo, *Angew. Chem. Int. Ed.* **2023**, *62*, e202303011.
- [100] Y. Ji, J. Xie, Z. Shen, Y. Liu, Z. Wen, L. Luo, G. Hong, *Adv. Funct. Mater.* **2023**, *33*, 2210043.
- [101] K. K. Sonigara, J. Zhao, H. K. Machhi, G. Cui, S. S. Soni, *Adv. Energy Mater.* **2020**, *10*, 2001997.
- [102] a) P. He, J. X. Huang, *Adv. Mater.* **2022**, *34*, 2109872; b) L. Wang, Z. Wang, H. Li, D. Han, X. Li, F. Wang, J. Gao, C. Geng, Z. Zhang, C. Cui, Z. Weng, C. Yang, K. P. Loh, Q. H. Yang, *ACS Nano* **2023**, *17*, 668; c) C. Ma, X. Wang, W. Lu, C. Wang, H. Yue, G. Sun, D. Zhang, F. Du, *Chem. Eng. J.* **2022**, *429*, 132576; d) W. Xin, J. Xiao, J. Li, L. Zhang, H. Peng, Z. Yan, Z. Zhu, *Energy Storage Mater.* **2023**, *56*, 76; e) S. H. Baek, J. S. Byun, H. J. Kim, S. J. Lee, J. M. Park, P. Xiong, Y. G. Chung, H. S. Park, *Chem. Eng. J.* **2023**, *468*, 143644.
- [103] P. Xiao, H. Li, J. Fu, C. Zeng, Y. Zhao, T. Zhai, H. Li, *Energy Environ. Sci.* **2022**, *15*, 1638.
- [104] T. Wei, X. Zhang, Y. Ren, Y. Wang, Z. Li, H. Zhang, L. Hu, *Chem. Eng. J.* **2023**, *457*, 141272.
- [105] R. Zhang, Y. Feng, Y. Ni, B. Zhong, M. Peng, T. Sun, S. Chen, H. Wang, Z. Tao, K. Zhang, *Angew. Chem. Int. Ed.* **2023**, *62*, e202304503.
- [106] a) C. C. Fan, W. J. Meng, D. S. Li, L. Jiang, *Energy Storage Mater.* **2023**, *56*, 468; b) Q. Wen, H. Fu, Y. Huang, R. Cui, H. Chen, R. Ji, L. Tang, C. Yan, J. Mao, K. Dai, Q. Wu, X. Zhang, J. Zheng, *Nano Energy* **2023**, *117*, 108810.
- [107] H. Lu, X. Zhang, M. Luo, K. Cao, Y. Lu, B. B. Xu, H. Pan, K. Tao, Y. Jiang, *Adv. Funct. Mater.* **2021**, *31*, 2103514.
- [108] R. Zhao, Y. Yang, G. Liu, R. Zhu, J. Huang, Z. Chen, Z. Gao, X. Chen, L. Qie, *Adv. Funct. Mater.* **2021**, *31*, 2001867.
- [109] Y. Li, D. Zhao, J. Cheng, Y. Lei, Z. Zhang, W. Zhang, Q. Zhu, *Chem. Eng. J.* **2023**, *452*, 139264.
- [110] Z. Hu, F. Zhang, Y. Zhao, H. Wang, Y. Huang, F. Wu, R. Chen, L. Li, *Adv. Mater.* **2022**, *34*, 2203104.
- [111] Z. Zhao, J. Zhao, Z. Hu, J. Li, J. Li, Y. Zhang, C. Wang, G. Cui, *Energy Environ. Sci.* **2019**, *12*, 1938.
- [112] G. Qian, G. Zan, J. Li, S. J. Lee, Y. Wang, Y. Zhu, S. Gul, D. J. Vine, S. Lewis, W. Yun, Z. F. Ma, P. Pianetta, J. S. Lee, L. Li, Y. Liu, *Adv. Energy Mater.* **2022**, *12*, 2200255.
- [113] K. Liang, S. Huang, H. Zhao, W. Liu, X. Huang, W. Chen, Y. Ren, J. Ma, *Adv. Mater. Interfaces* **2022**, *9*, 2200564.
- [114] D. Lee, H. I. Kim, W. Y. Kim, S. K. Cho, K. Baek, K. Jeong, D. B. Ahn, S. Park, S. J. Kang, S. Y. Lee, *Adv. Funct. Mater.* **2021**, *31*, 2103850.
- [115] a) Y. Liu, J. Hu, Q. Lu, M. Hantusch, H. Zhang, Z. Qu, H. Tang, H. Dong, O. G. Schmidt, R. Holze, M. Zhu, *Energy Storage Mater.* **2022**, *47*, 98; b) X. Ni, J. Zhou, H. Ji, Y. Chen, H. Yu, Y. Zheng, T. Qian, M. Wang, L. Chen, C. Yan, *Adv. Funct. Mater.* **2023**, *33*, 2302293; c) T. Liu, J. Hong, J. Wang, Y. Xu, Y. Wang, *Energy Storage Mater.* **2022**, *45*, 1074; d) P. Xiao, Y. Wu, K. Liu, X. Feng, J. Liang, Y. Zhao, C. Wang, X. Xu, T. Zhai, H. Li, *Angew. Chem. Int. Ed.* **2023**, *62*, e202309765.
- [116] a) R. Zhang, Y. Feng, Y. Ni, B. Zhong, M. Peng, T. Sun, S. Chen, H. Wang, Z. Tao, K. Zhang, *Angew. Chem. Int. Ed.* **2023**, *62*, e202304503; b) J. Ren, C. Li, P. Li, S. Liu, L. Wang, *Chem. Eng. J.* **2023**, *462*, 142270; c) Q. Zong, B. Lv, C. Liu, Y. Yu, Q. Kang, D. Li, Z. Zhu, D. Tao, J. Zhang, J. Wang, Q. Zhang, G. Cao, *ACS Energy Lett.* **2023**, *8*, 2886.
- [117] C. Tian, J. Wang, R. Sun, T. Ali, H. Wang, B. B. Xie, Y. Zhong, Y. Hu, *Angew. Chem. Int. Ed.* **2023**, *62*, e202310970.
- [118] L. Zhang, B. Zhang, T. Zhang, T. Li, T. Shi, W. Li, T. Shen, X. Huang, J. Xu, X. Zhang, Z. Wang, Y. Hou, *Adv. Funct. Mater.* **2021**, *31*, 2100186.

Manuscript received: October 18, 2023

Revised manuscript received: November 23, 2023

Accepted manuscript online: November 27, 2023

Version of record online: December 13, 2023